Seismogenesis of dual subdution beneath Kanto, central Japan controlled by fluid release

Yingfeng JI[1], Shoichi YOSHIOKA[1,2],
Vlad C. MANEA[3] and Marina MANEA[3]

1 RCUSS, Kobe University, Japan

2 Graduate School of Science, Kobe University, Japan

3 UNAM, Mexico

Tectonic map

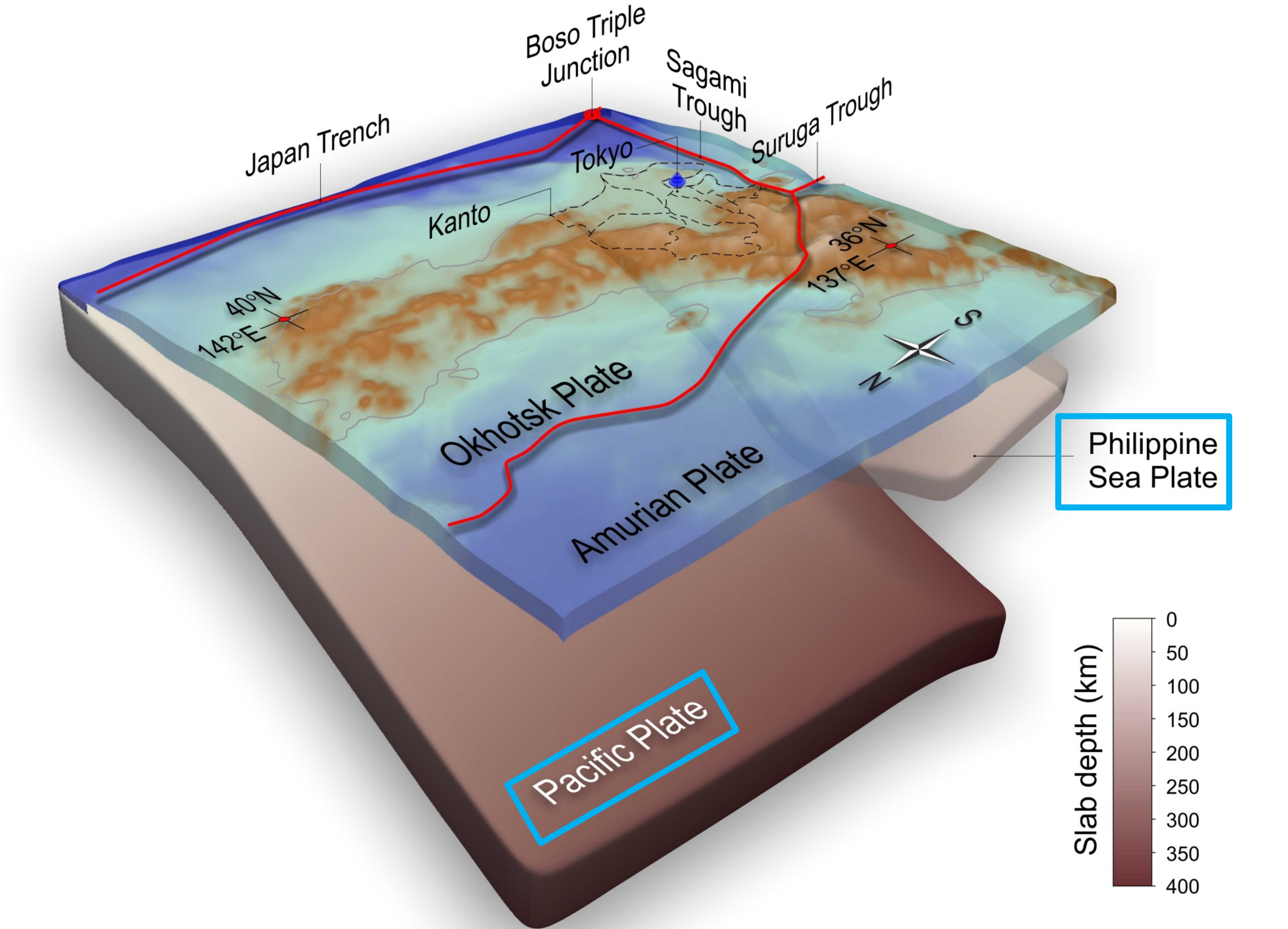

Plate geometry model

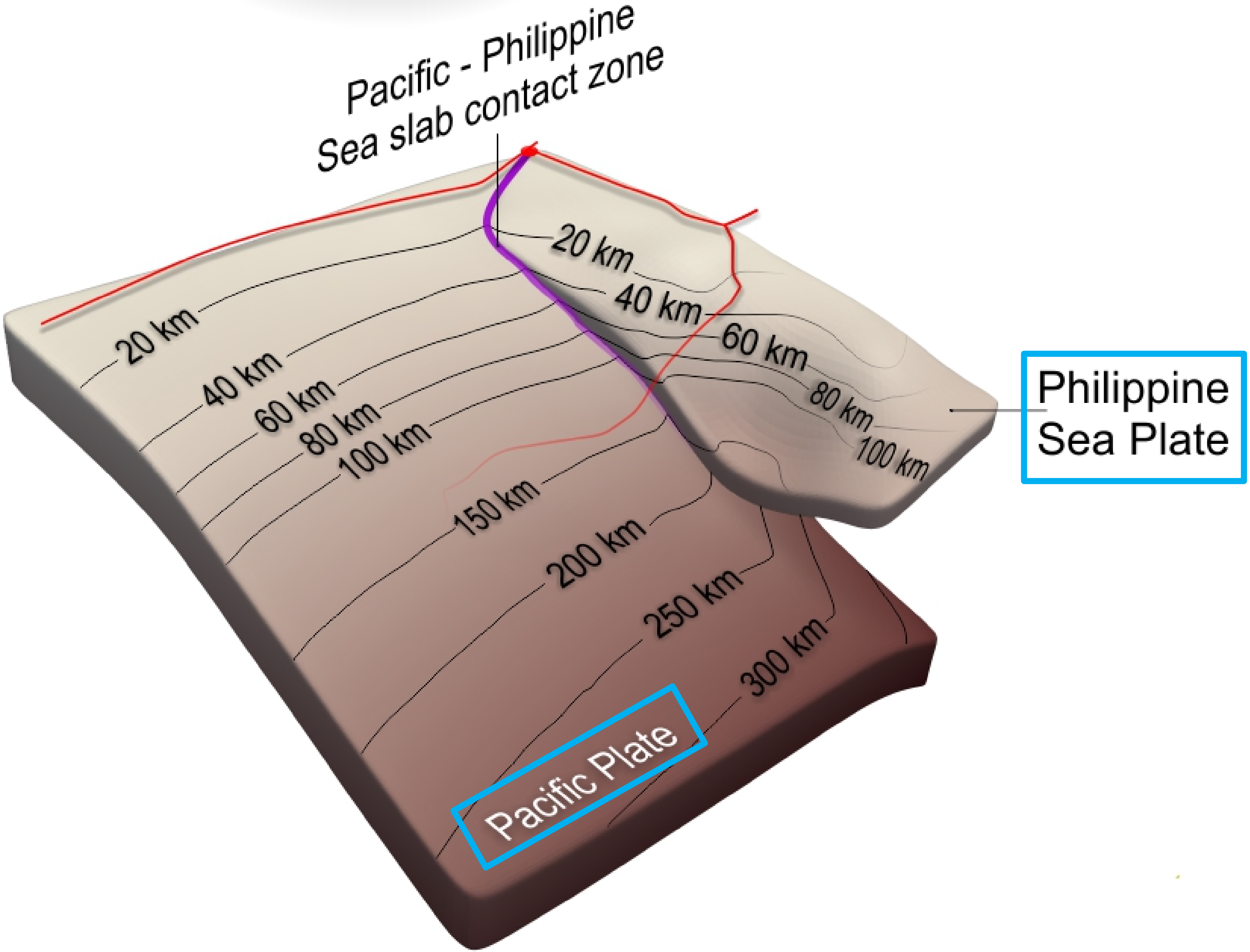

Seismogenic zone in and around the PAC slab interface

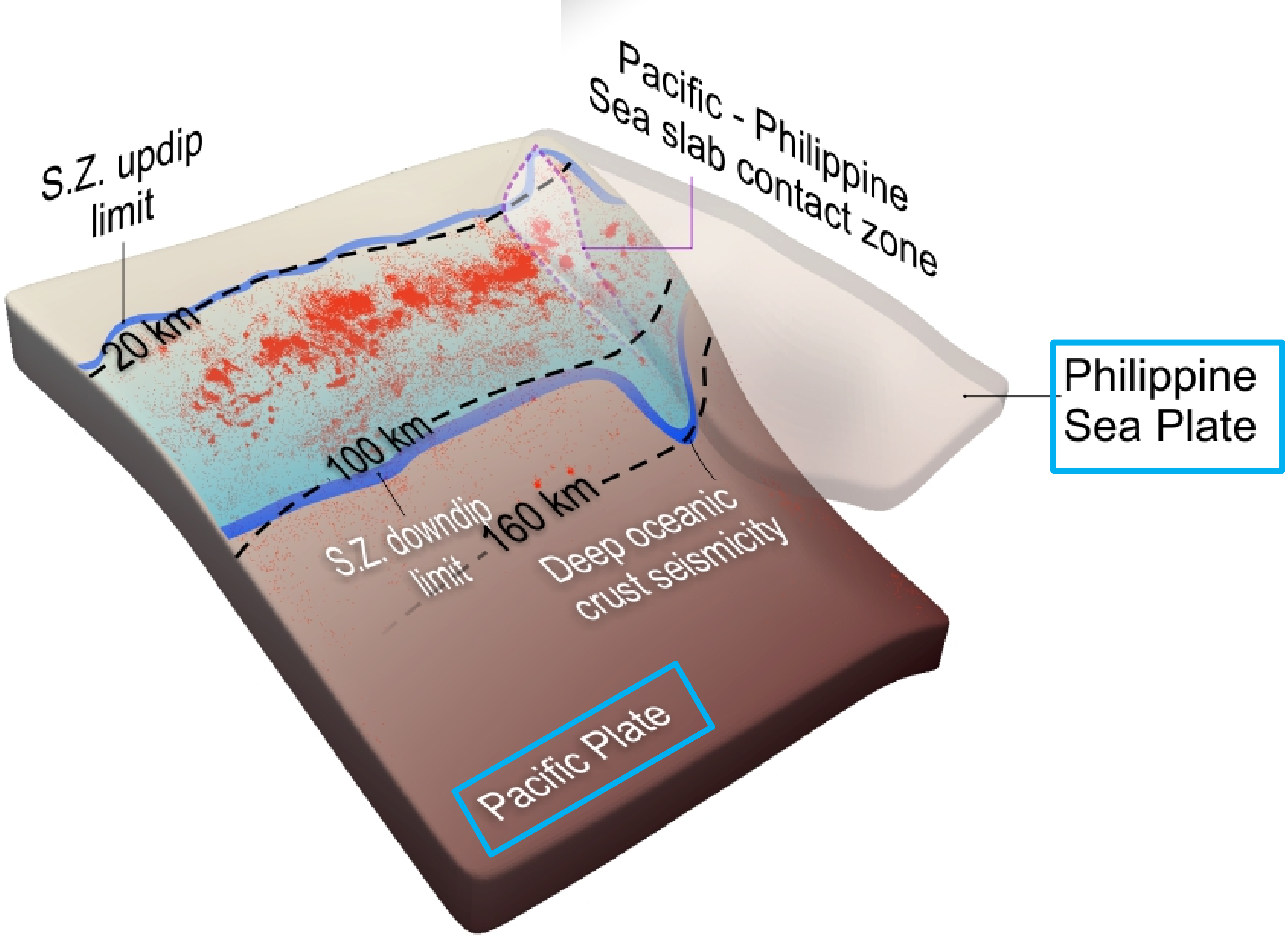

Objectives

- To understand the effect of existence of the PHS slab on geodynamic process beneath Kanto, central Japan (thermal structure, dehydration, and mantle flow)

- To elucidate seismogenesis of inter- and intra-plate earthquakes (≧M2) of the PAC slab, especially deepening of the seismogenic zone at the down-dip side of the slab-slab contact zone

Previous study

- 2-D model
  - Iwamori (EPSL, 2000)
  - Yoshioka et al. (GJI, 2015)
- 3-D model
  - Wada and He (GRL, 2017)

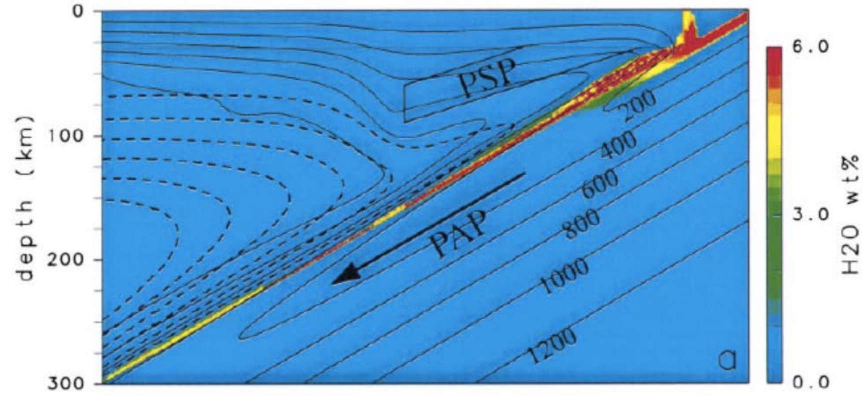

Iwamori (EPSL, 2000)

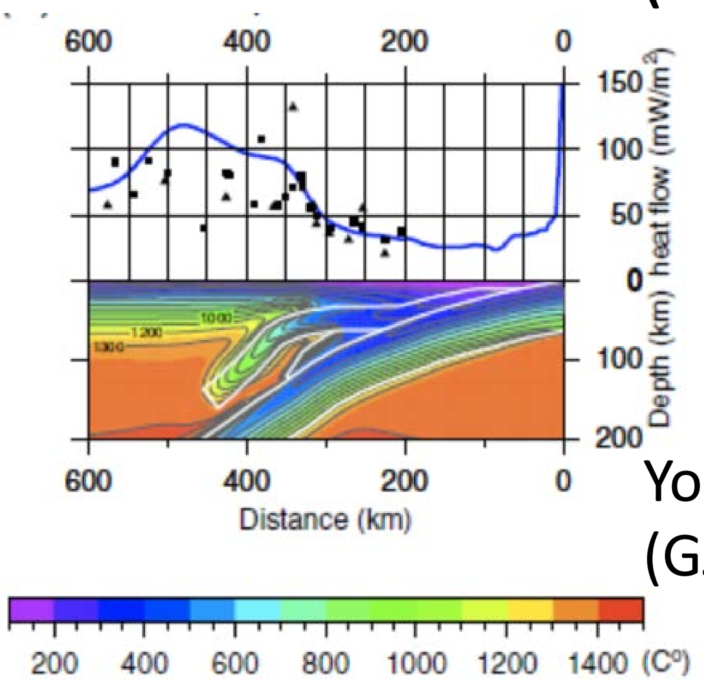

Yoshioka et al. (GJI, 2015)

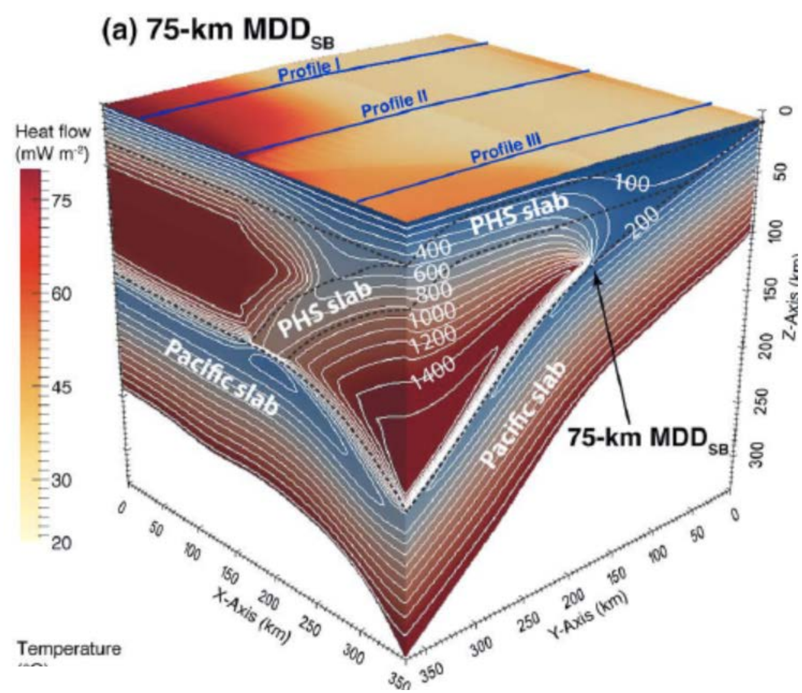

Wada and He (GRL, 2017)

What's new ?

- 3-D
- time dependent
- subduction history
- a moving prescribed guide
- high-density heat flow data
- relationship between dehydration and inter- & intra-plate seismicity of the PAC slab, using phase diagrams of hydrous minerals

Geometry of the upper surfaces of the Pacific and the Philippine Sea slabs

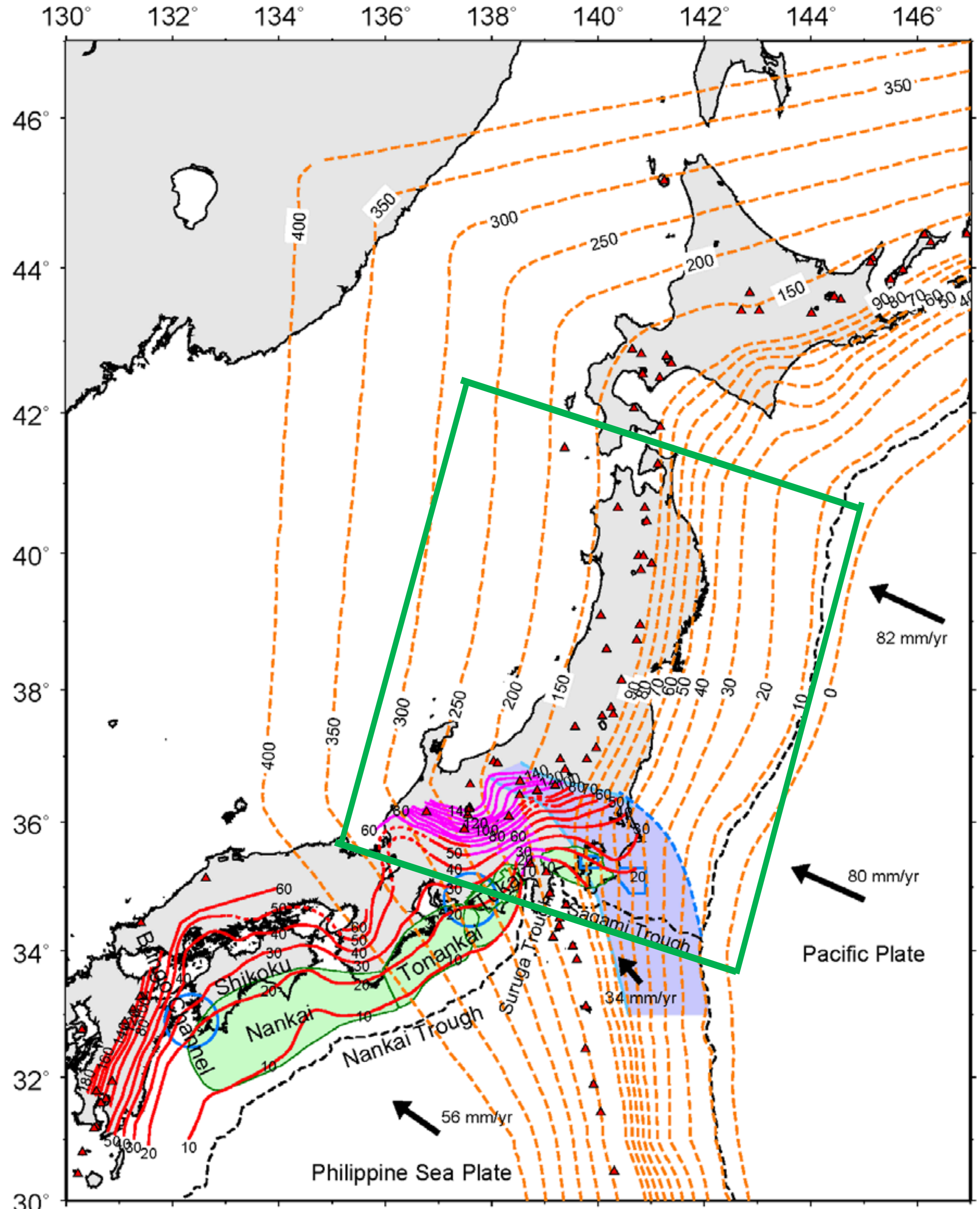

Nakajima and Hasegawa (2006, 2009)
Kita et al. (2010)

Model setting

Imposed temperature distribution at the seaward boundaries

$$T = T_0 + (T_1 - T_0)\left[\frac{z}{d_l} + \frac{2}{\pi}\sum_{n=1}^{\infty}\frac{1}{n}\exp\left(-\frac{\kappa n^2 \pi^2 t}{d_l^{\,2}}\right)\sin\left(\frac{n\pi z}{d_l}\right)\right]$$

$T_1 = 1402^{\circ}\mathrm{C}$

$d_l = 134.9\mathrm{km}$

age

RT 1 model (Grose, 2012)

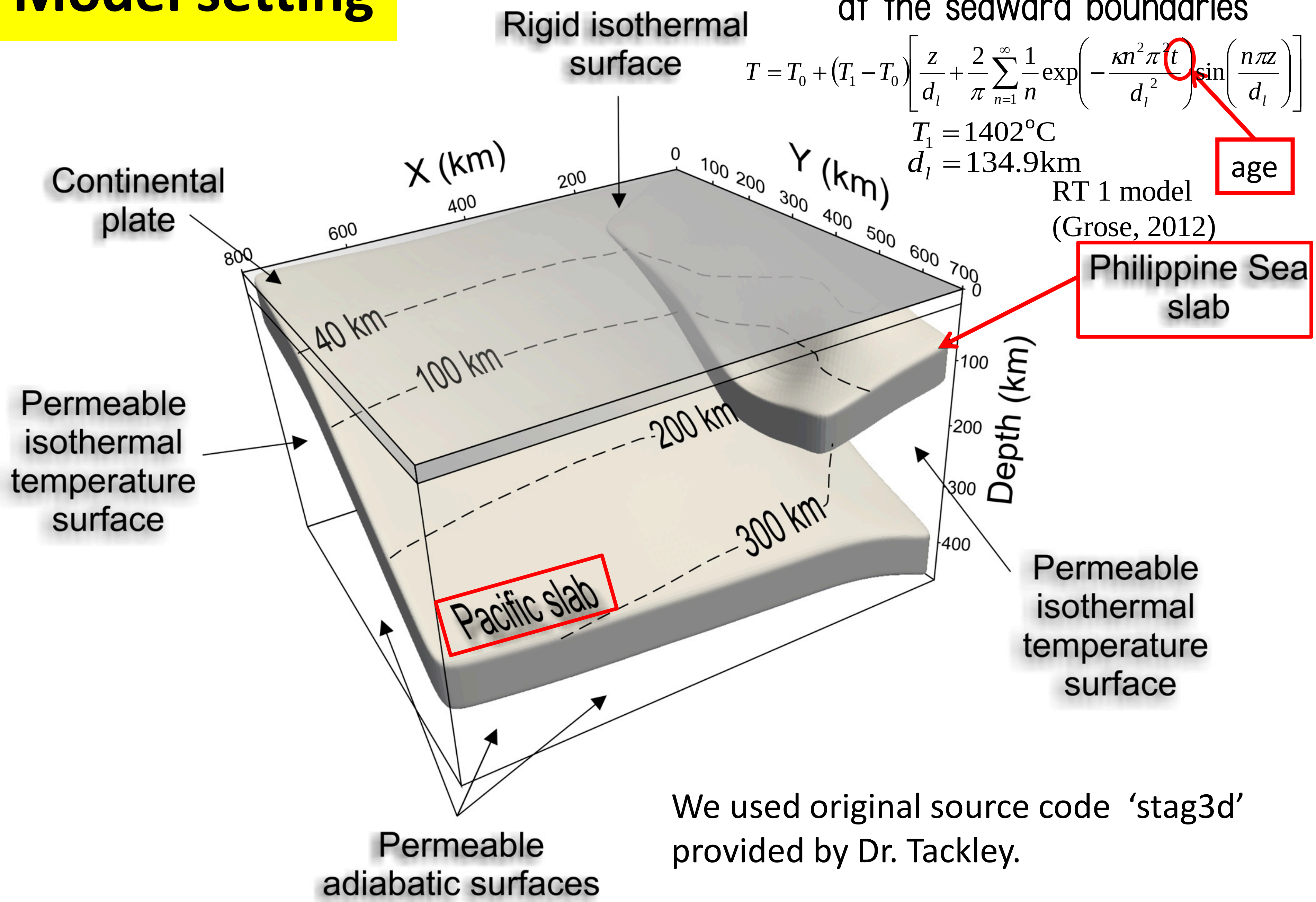

We used original source code ‘stag3d’ provided by Dr. Tackley.

Phase diagram of water content for hydrous minerals included in a slab

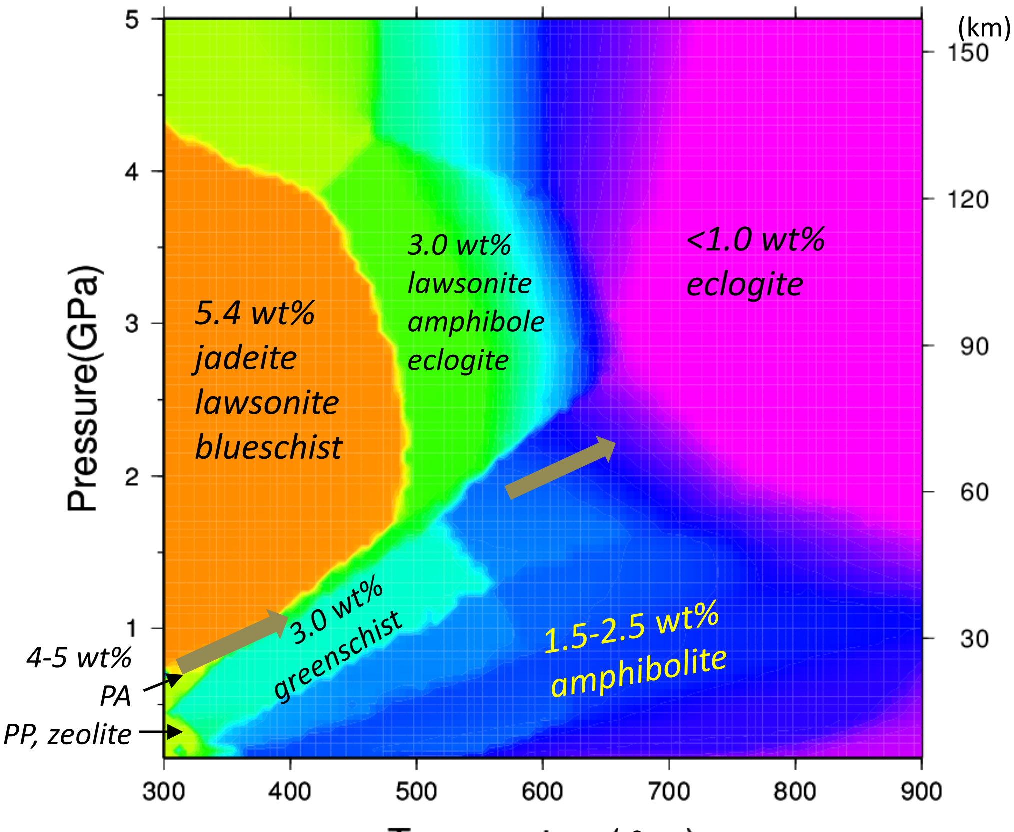

PA: pumpellyite actinolite
PP: prehnite pumpellyite

Omori et al. (2009)

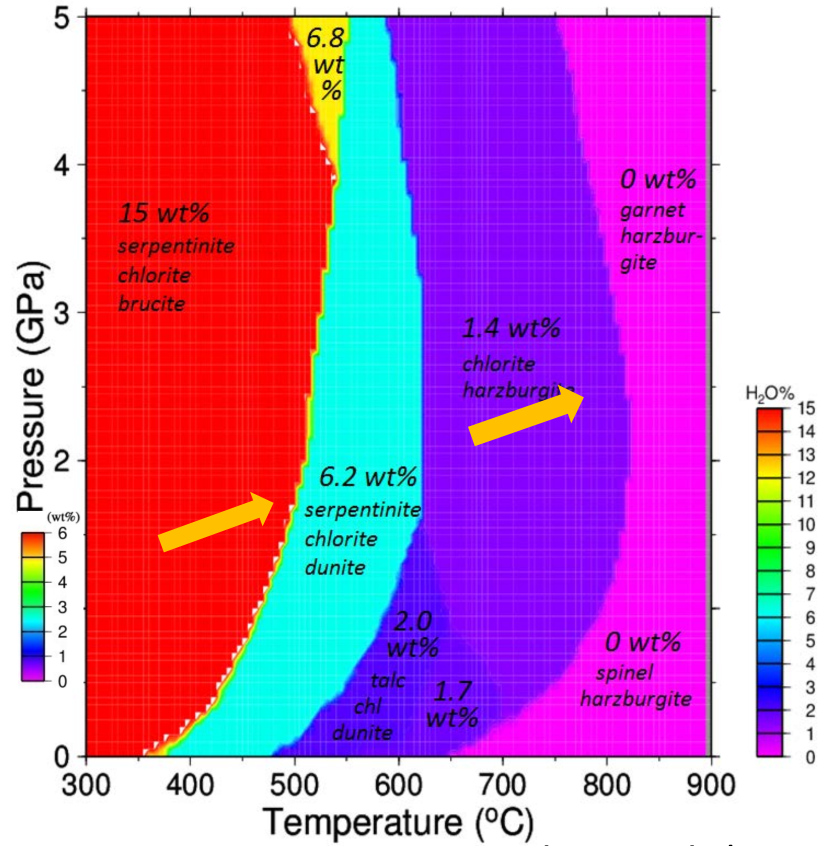

Hacker et al. (2003)

hydrous MORB

PA(pumpellyite actinolite) (4-5wt%)

(-1.5 - -2.5wt%) ➡ *greenschist (3.0wt%)*

(-0.5 - -1.5wt%) ➡ *amphibolite (1.5-2.5wt%)*

(-1.5 - -2.5wt%) ➡ *eclogite (0wt%)*

ultramafic rock (harzburgite)

serpentinite chlorite brucite (15wt%)

(-9 wt%) ➡ *serpentinite chlorite dunite (6.2wt%)*

(-5 - -6wt%) ➡ *harzburgite (0-1.4 wt%)*

Distributions of temperature and water content on the upper surfaces of the slabs beneath Kanto

Pacific slab alone

Pacific slab ＋ Philippine Sea slab

temperature distribution

water content distribution

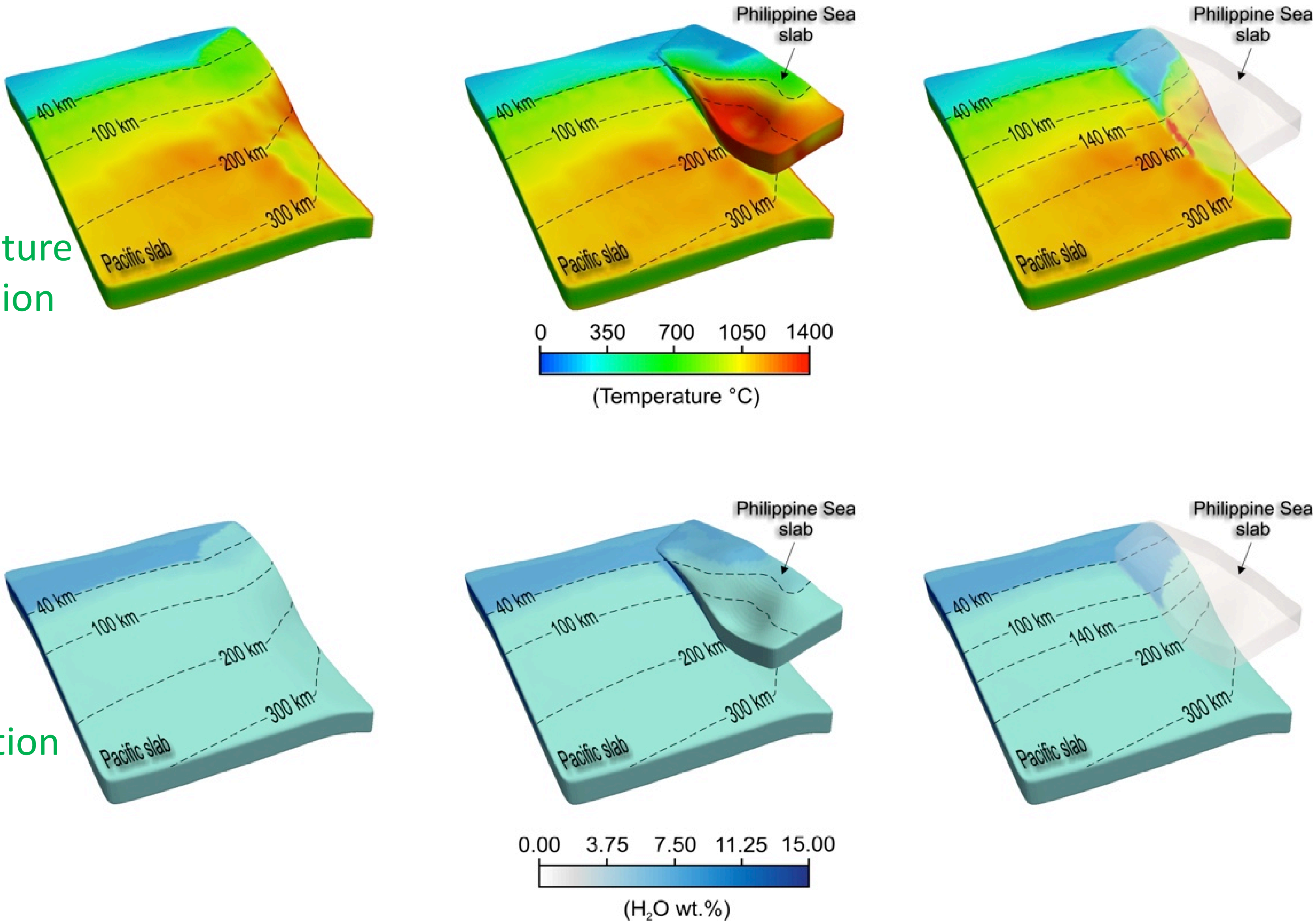

Thermal structure on the upper surface of the slabs and flow pattern in the mantle wedge beneath Kanto

Pacific slab alone

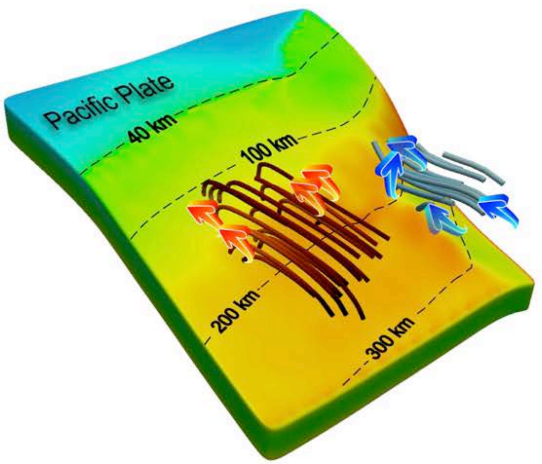

Pacific slab ＋ Philippine Sea slab

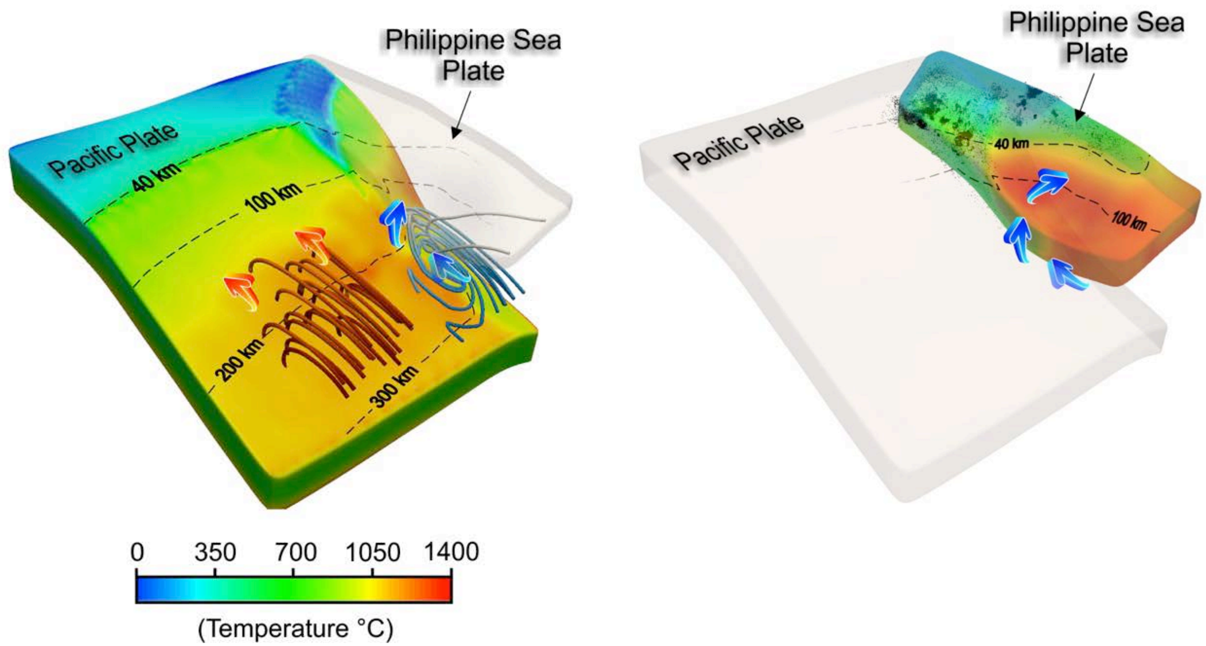

Distributions of temperature and water content in the Pacific slab at different depths beneath Kanto

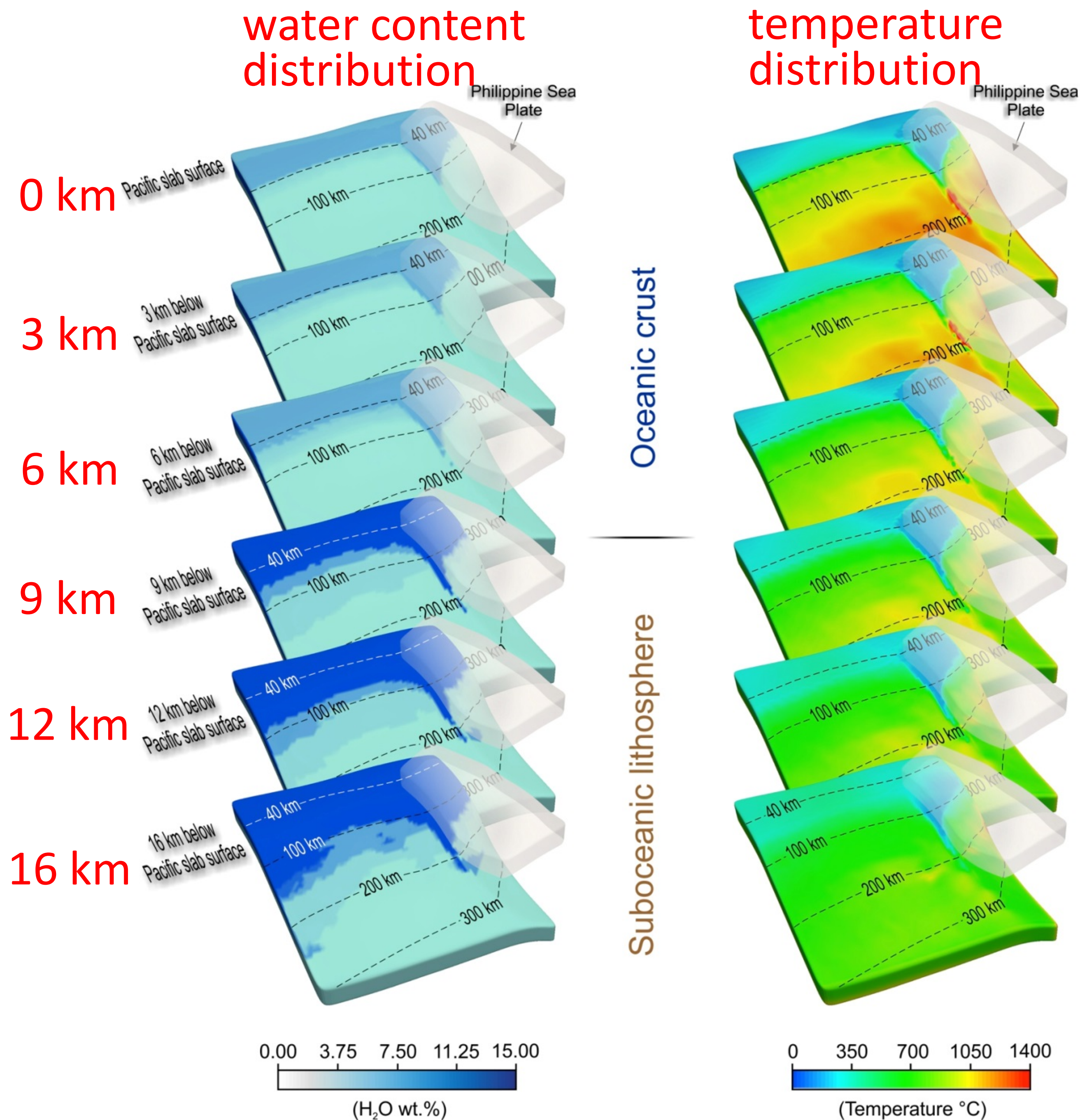

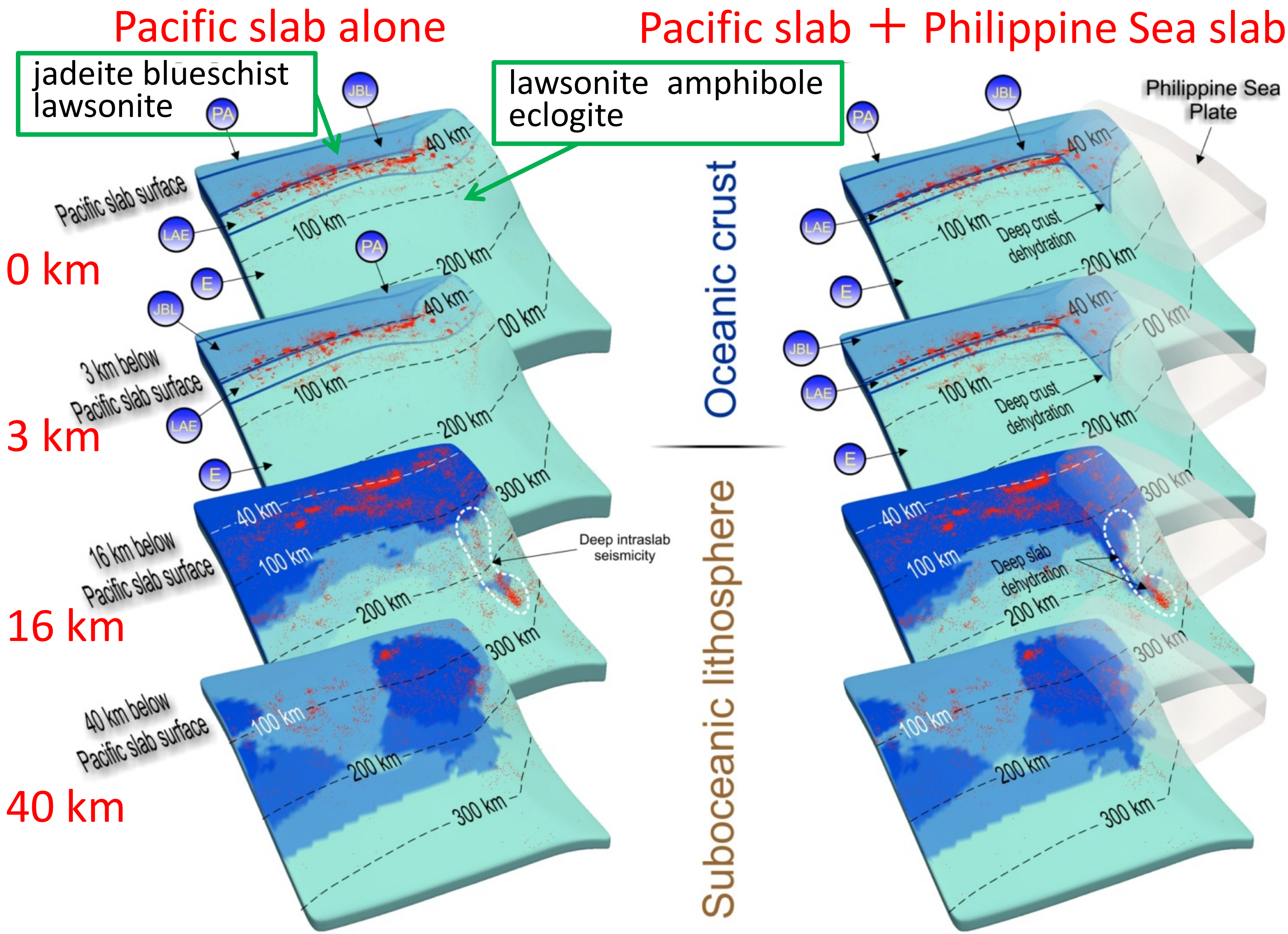

Seismicity and water content distributions in the Pacific slab at different depths beneath Kanto

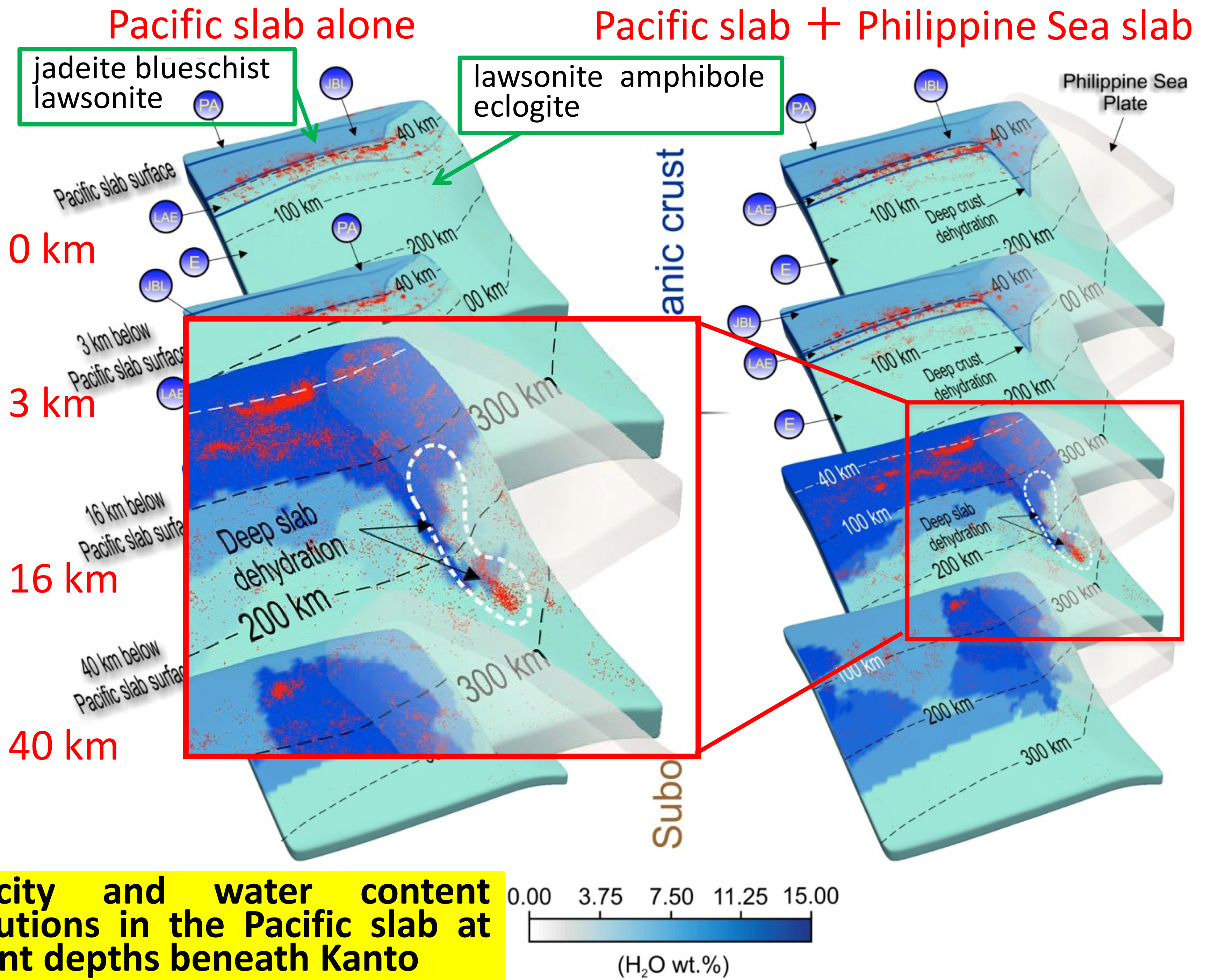

Seismicity and water content distributions in the Pacific slab at different depths beneath Kanto

Conclusions

- Constructed 3-D high-resolution thermal structure model associated with dual subduction beneath Kanto.

- Seismicity in the oceanic crust in the PAC slab (at depths of about 40 km) corresponds well to dehydrated area associated with the phase transformation.

- The effect of existence of the PHS slab on distributions of temperature, dehydration, and seismicity in the PAC slab
  - → Temperature decreases at the slab-slab contact zone
  - → Water is carried to the deeper portion there in a form of OH group due to delay of phase transformations
  - → Water released area at the deeper portion of the contact zone coincides well with intraslab deep seismicity

Thank you for your attention

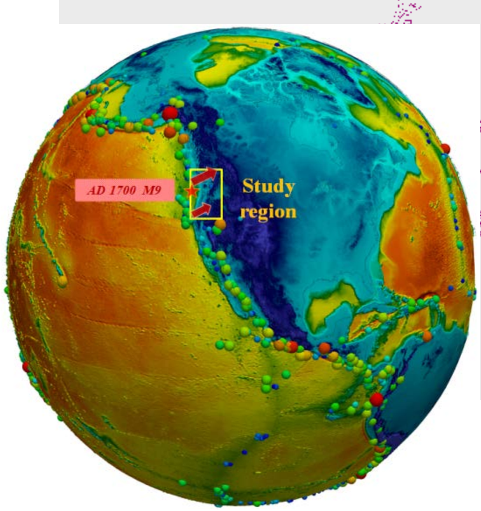

This presentation is based on
Ji et al., Scientific Reports, 7, 16864 (2017)

Method

Governing equations for 3-D parallelepiped thermal convection model

Mass conservation

$$\nabla \cdot [\rho_s(z)\mathbf{v}] = 0$$

anelastic liquid approximation

Momentum equation

$$-\frac{\partial P}{\partial x_i} + \frac{\partial \tau_{ij}}{\partial x_j} + \delta_{i3}\rho_s g \alpha_0 (T - T_s) = 0$$

Energy equation

$$\rho c_p\left(\frac{\partial T}{\partial t} + \underline{v \cdot \nabla T}\right) = \underline{k\nabla^2 T} + \underline{\eta(\nabla v)^2} + \underline{\rho g a T v} + \underline{H_r \rho} + \underline{\tau \dot{\varepsilon}}$$

advection **conduction** **viscous dissipation** **adiabatic heating** **radioactive heating** **frictional heating on the plate interface**

Viscosity

$$\eta = \frac{\eta_{diff}\eta_{disl}}{\eta_{diff} + \eta_{disl}} \qquad \eta_{diff,disl} = \left(\frac{d^p}{AC_{OH}^r}\right)^{\frac{1}{n}} \dot{\varepsilon}^{(1-n)/n} \exp\left[\frac{E + P_{lc}V}{nRT}\right]$$

Burkett and Billen (2010)

Age of the Pacific and the Philippine Sea plates

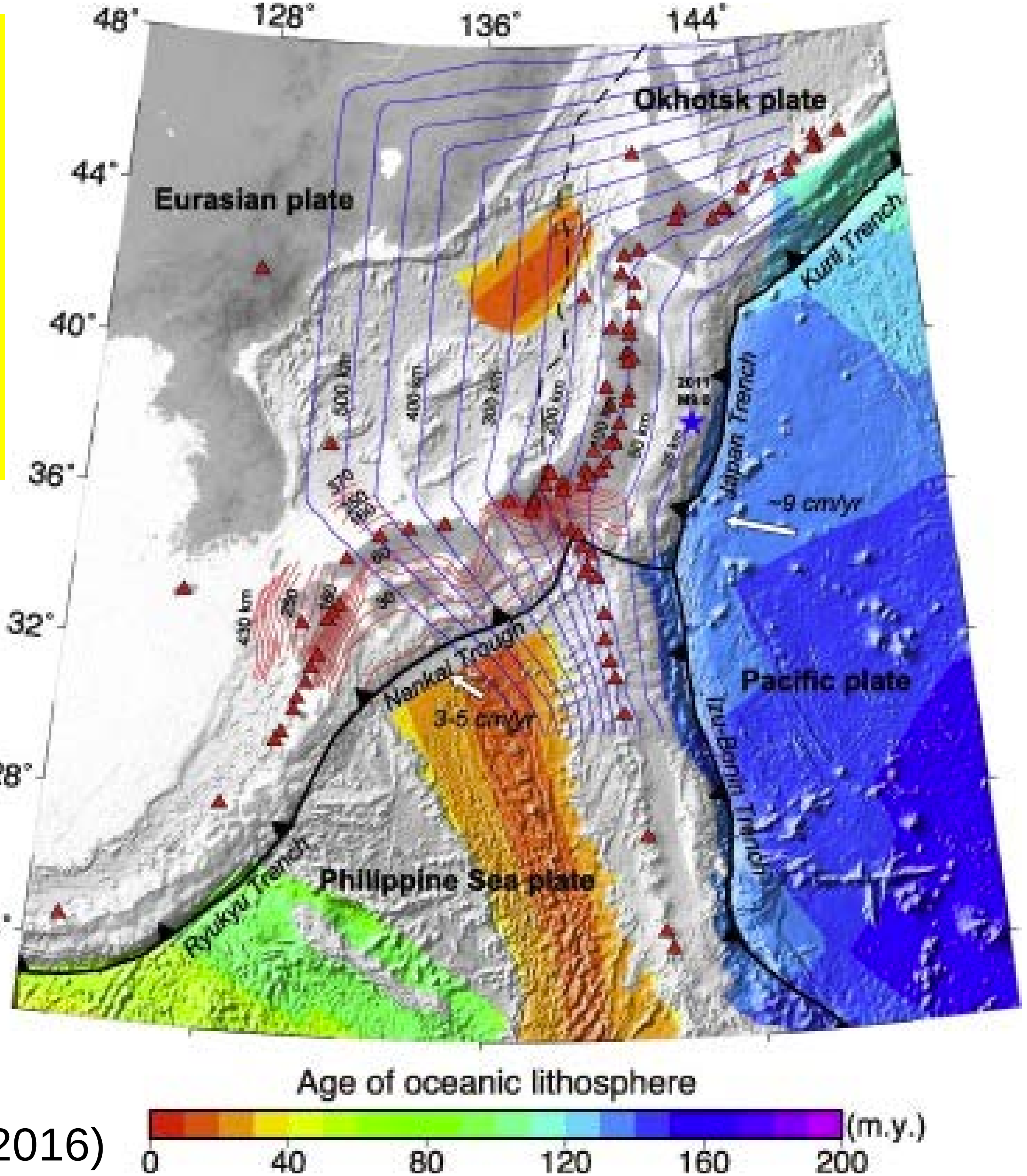

Image from Liu and Zhao (2016)

Subduction history of the Pacific and the Philippine Sea plates from 20 Ma to the present

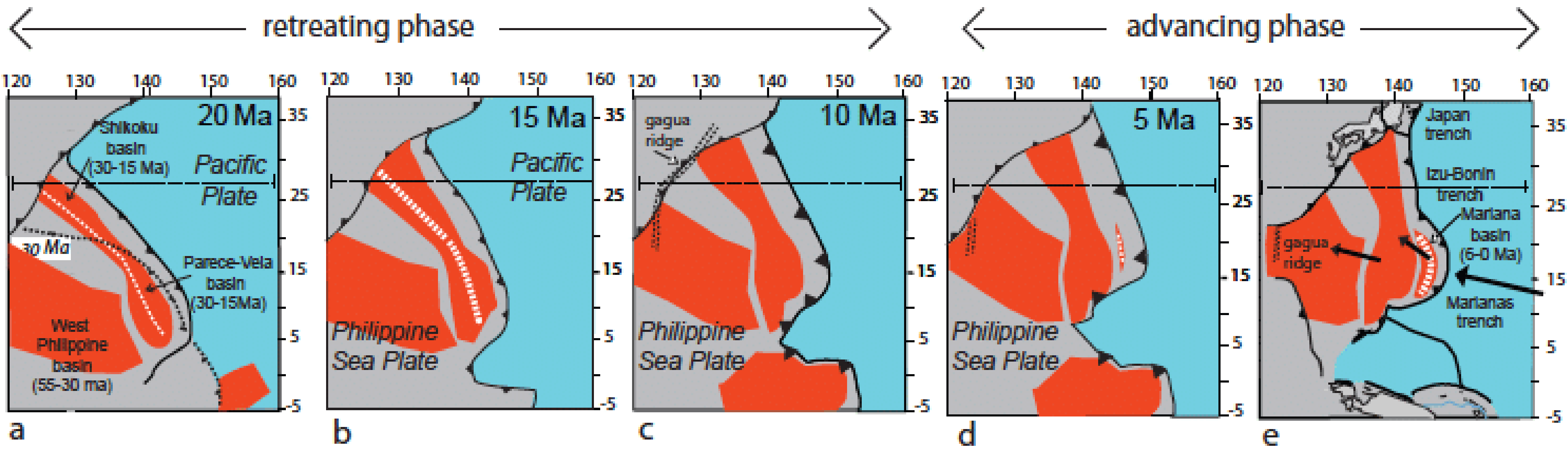

Hall et al. (1995); Faccenna et al. (2017)

Heat flow distribution

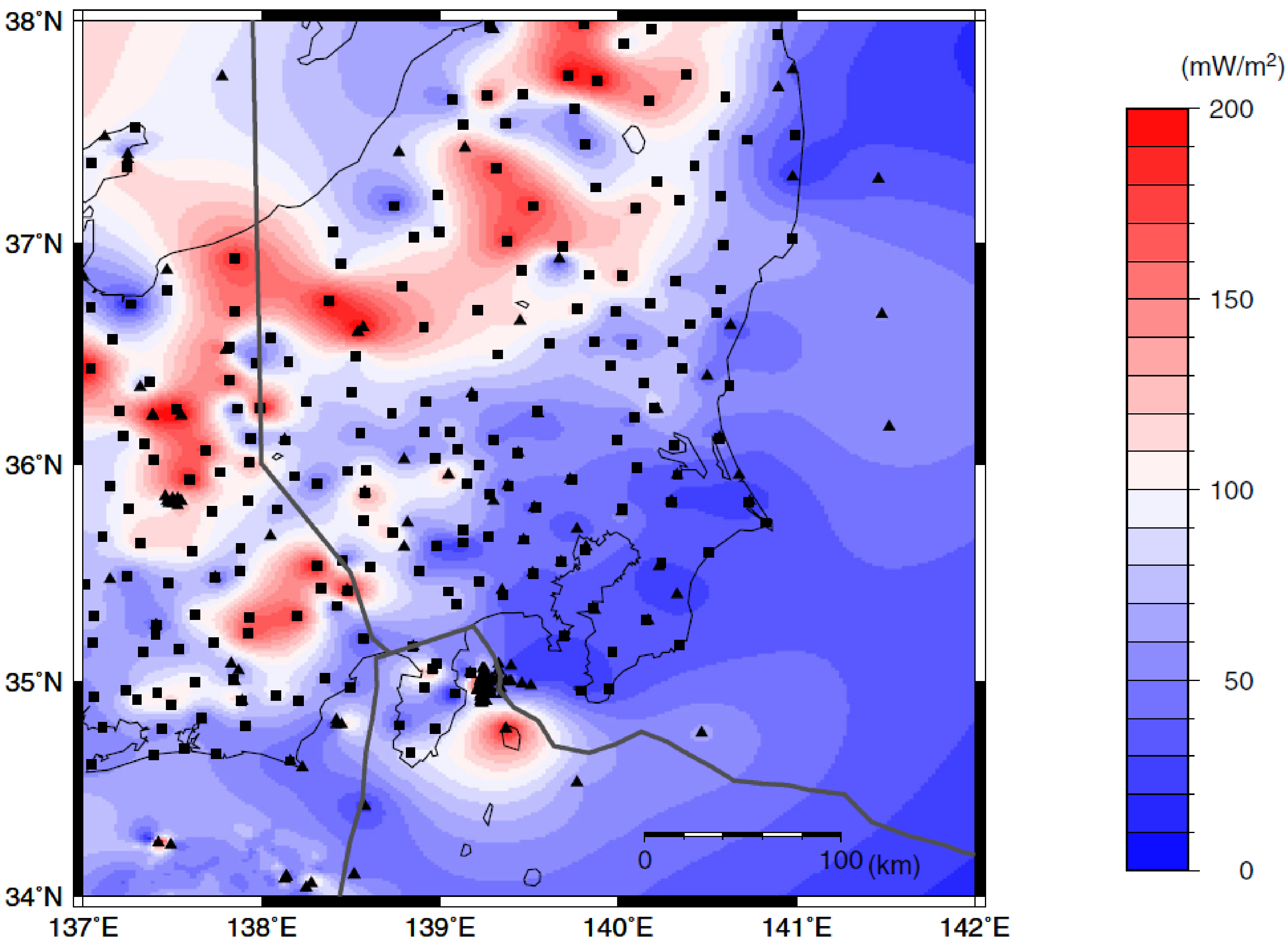

Yoshioka et al. (2015)

Parameters in our 3D Modeling

Symbol	Parameters	Value	Units
ρ_0	Standard density	3300[1]	kg/m^3
T_0	Temperature difference between top and bottom of model	1600	K
k_0	Standard thermal conductivity	2.9[3]	w/mK
Hr	Radioactive heat generation rate in the mantle	2.245×10^{-13}	w/m^3
C_{p_0}	Standard specific heat at constant pressure	1200 [1]	J/kgK
κ_0	Standard thermal diffusivity	7.6×10^{-7} [4]	m^2/s
η_0	Standard viscosity	10^{20} [3]	$Pa\cdot s$
α_0	Standard thermal expansion	3×10^{-5} [2]	$/K$
v_1	Straight subduction velocity	4.0[1]	cm/yr
v_2	Oblique subduction velocity	6.3[5]	cm/yr

(1) Wang et al. (1995) (2) Iwamori (1997) (3) Christensen (1996) (4) Yoshioka & Murakami. (2007) (5) Sella et al (2002)

Table 1. Thermal properties used for the temperature calculations.

Geological unit	Thermal conductivity $Wm^{-1}\,k^{-1}$	Heat production ($W\,k^{-1}$)	Density ($kg\,m^{-3}$)
Upper crust (0–16 km)	2.5^{a}	7.3×10^{-10a}	2600^{a}
Lower crust (16–32 km)	2.5^{a}	1.4×10^{-10a}	2900^{a}
Mantle and oceanic plate	2.5	2.245×10^{-13a}	3300^{a}
Accretionary prism	1.4^{b}	7.3×10^{-10a}	2600^{a}

[a] Wang *et al.* (1995).

[b] Ashi *et al.* (2002).

$$\eta_{comp} = \frac{\eta_{df}\eta_{ds}}{\eta_{df} + \eta_{ds}}.$$

$$\eta_{df,ds} = \left(\frac{d^p}{A_0 C_{OH}^r}\right)^{\frac{1}{n}} \dot{\varepsilon}_E^{\frac{1-n}{n}} \exp\left(\frac{E_0 + P_l V_0}{n_0 R T_a}\right),$$

	Flow law parameters		
	Parameter	Diffusion creep	Dislocation creep
n_0	Stress exponent	1.0	3.5
A_0	Preexponential factor ($s^{-n}Pa^{-n}\mu m^{p}H^{-r}\ 10^{6r}Si^{r}$)	1.0	9.0×10^{-20}
E_0	Activiation energy (kJ/mol)	335	480
V_0	Activiation volume (m^3/mol)		
	Upper mantle	4.0×10^{-6}	11.0×10^{-6}
	Lower mantle	1.5×10^{-6}	-
d	Grain size (μm)		
	Upper mantle	10,000	-
	Lower mantle	40,000	-
p	Grain size exponent	3.0	-
C_{OH}	OH concertration ($H/10^6Si$)	1000	1000
r	C_{OH} exponent	1.0	1.2

Model parameters for the diffusion and dislocation creep of olivine (Armienti and Tarquini, 2002; Hirth and Kohlstedt, 2003; Burkett and Billen, 2010)

The model parameters (Table 2) were tested for sensitivity by changing them by ±5 per cent, and changes in the 150, 350 and 450 °C isotherm locations were determined (Fig. 10). A change of ±65 °C in ΔT, which contributes to Ra_0, ξ and Rh_0, changed the average locations of the eight profiles by ∓2, ∓9 and ∓12 km, respectively. Changing mantle thermal diffusivity, defined by ρ, k and Cp, by $\pm 3.2 \times 10^{-8}$ m^2 s^{-1} moved the average locations by ∓1, ∓4 and ∓3 km, respectively. Changes in D, Rh_{mantle} and α_0, which also affect Di_0, Γ_0 and ξ, had negligible effects on the average locations. If the continental Moho depth was 30 km, which was 2 km shallower than the depth used in this model, the average locations would change by ∓0, ∓0 and ∓3 km, respectively. We used

Temperature and H_2O variations for mantle density variation of -50 kg/m^3 (mantle density of 3250 kg/m^3)

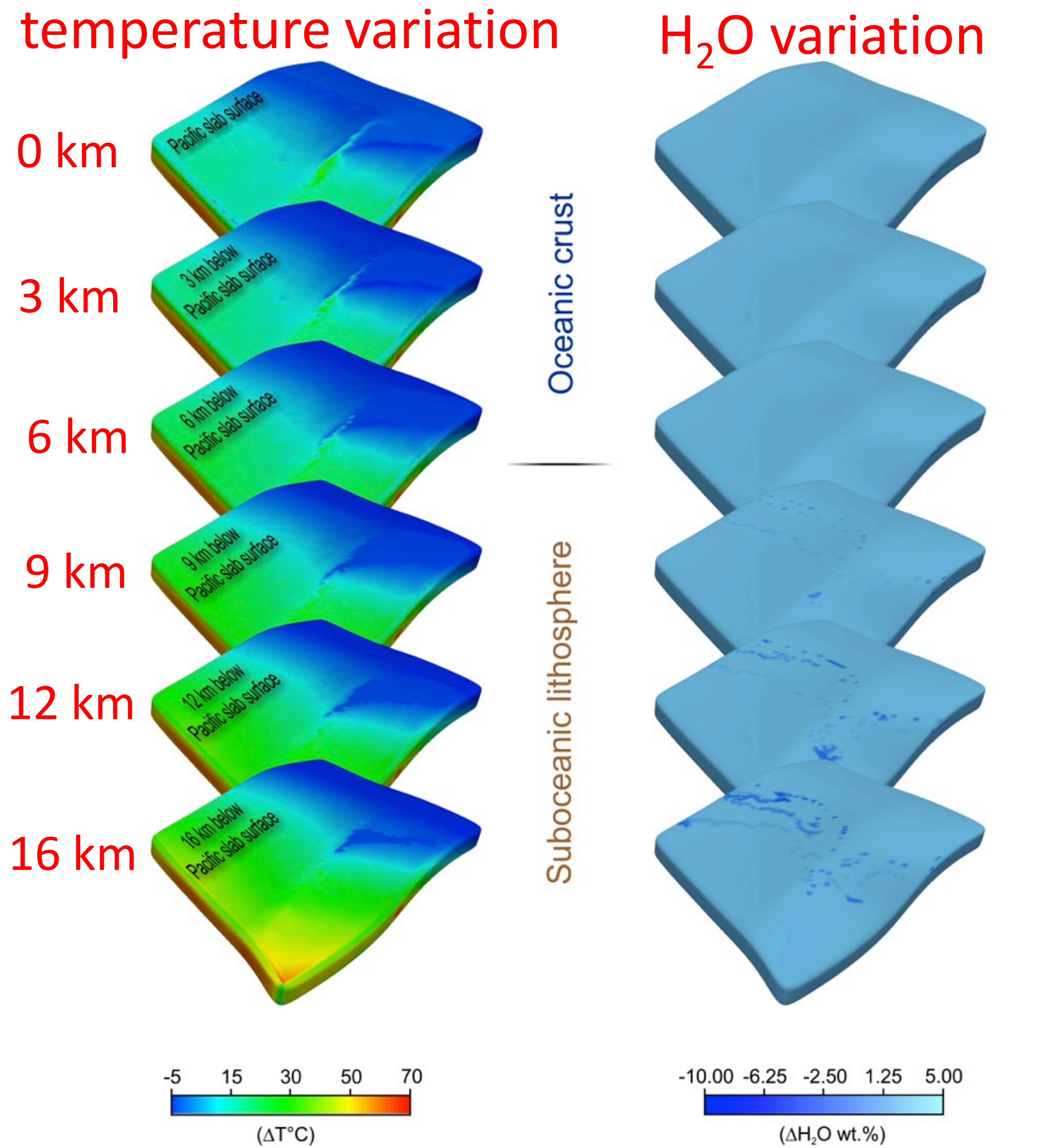

Temperature and H_2O variations for mantle density variation of +50 kg/m^3 (mantle density of 3350 kg/m^3)

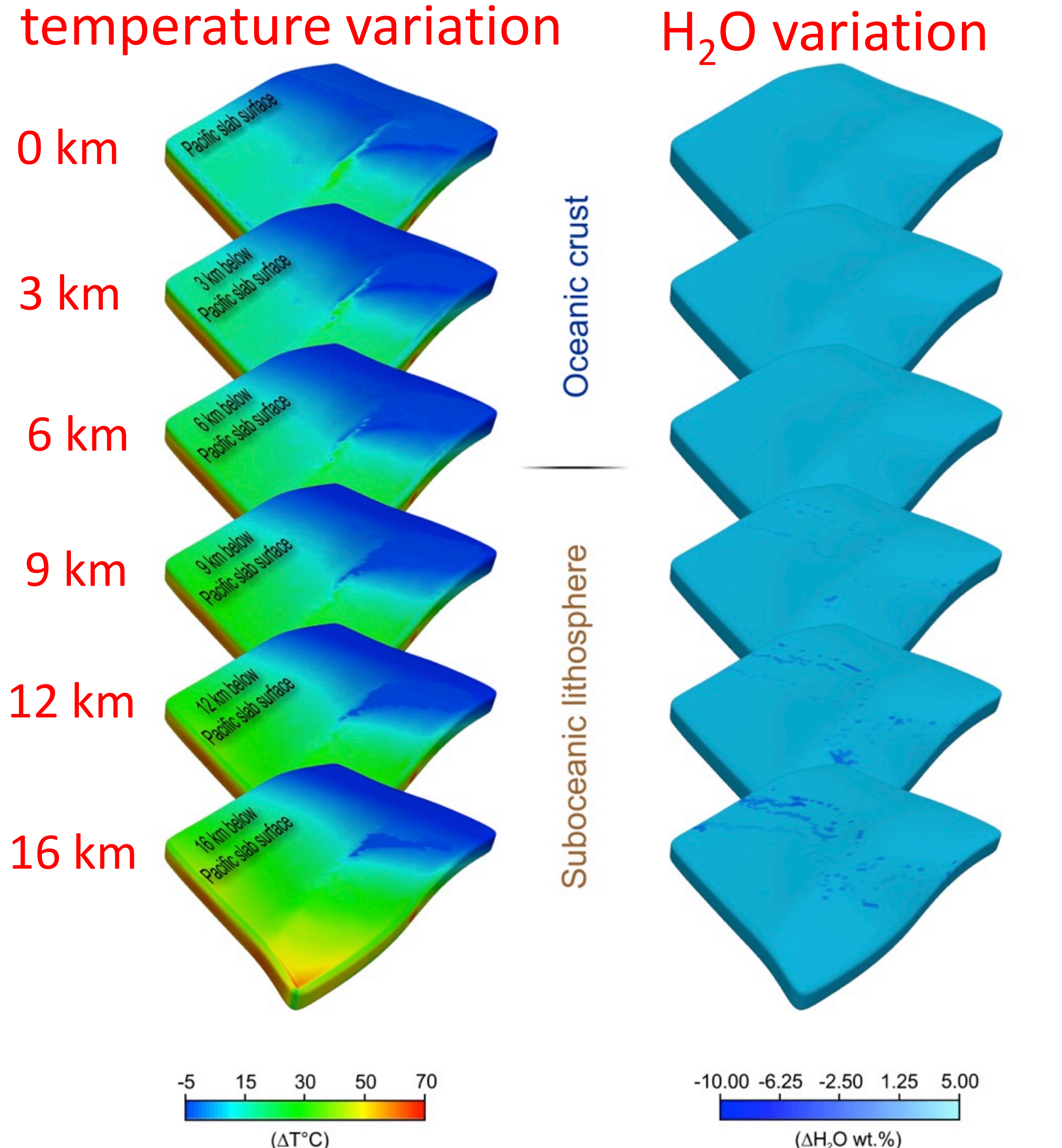

Temperature and H_2O variations for mantle viscosity variation of $-0.1x10^{20}$ Pa s (mantle viscosity of $0.9x10^{20}$ Pa s)

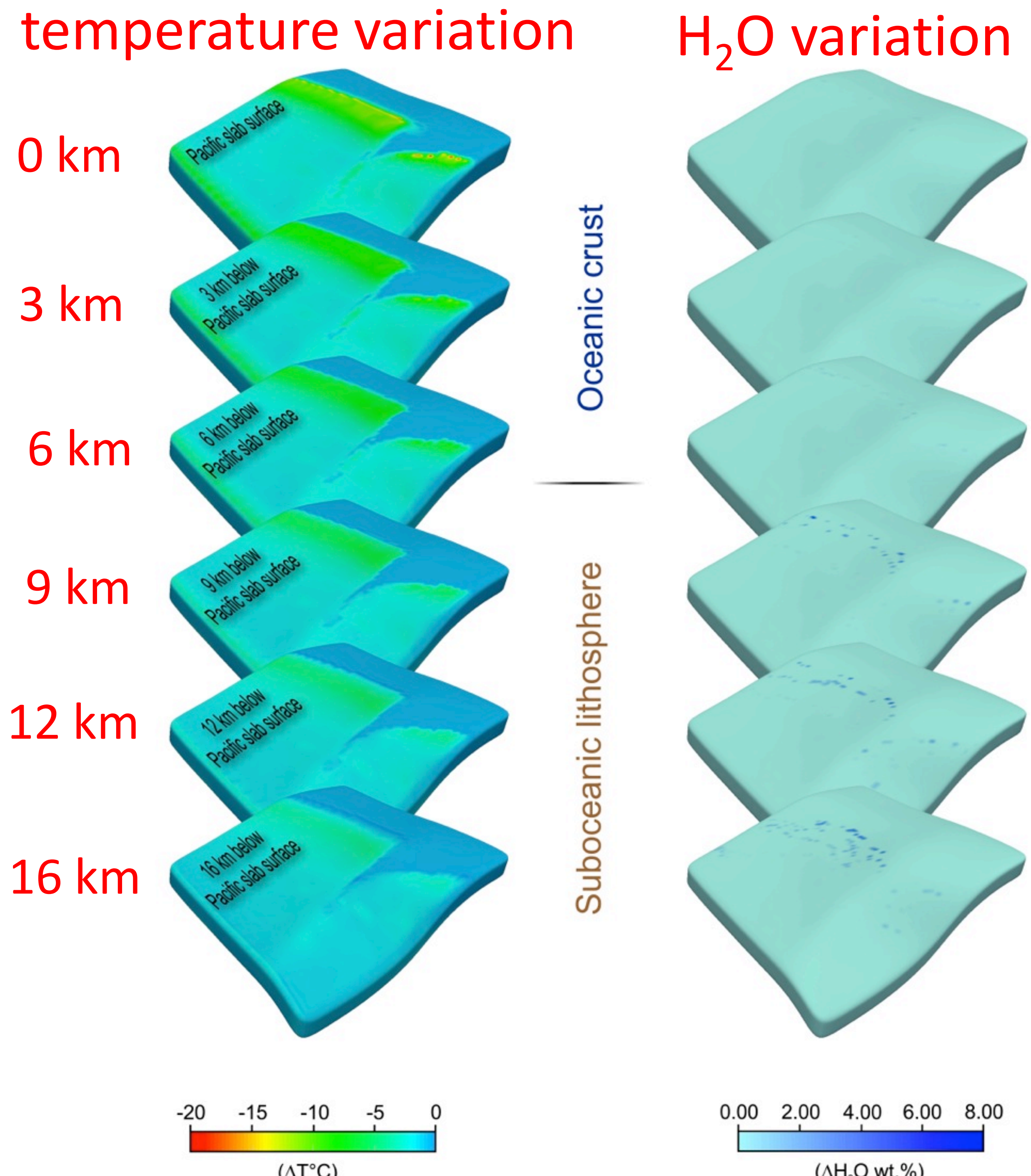

Temperature and H_2O variations for mantle viscosity variation of $+0.1x10^{20}$ Pa s (mantle viscosity of $1.1x10^{20}$ Pa s)

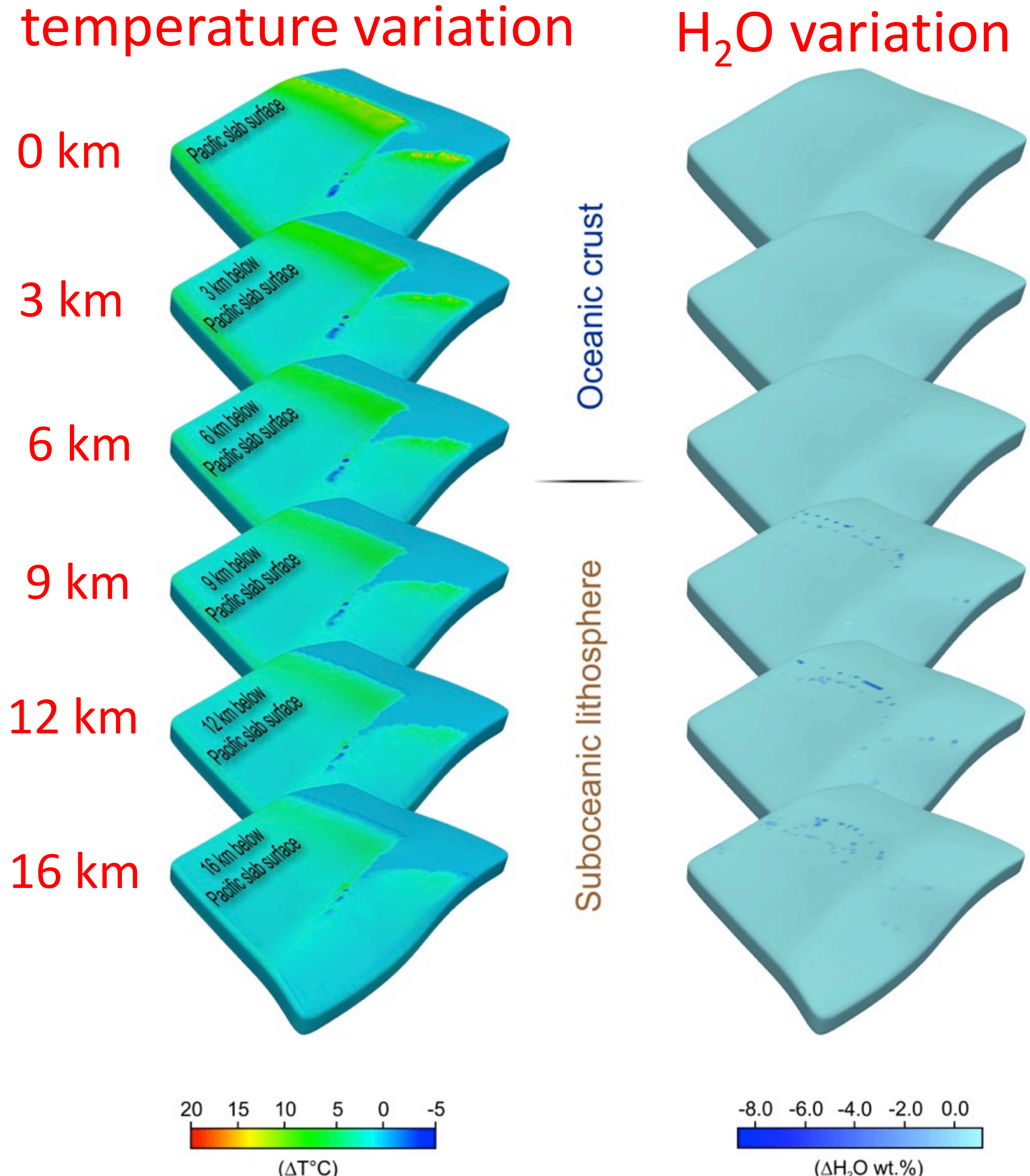

Tectonic map (1)

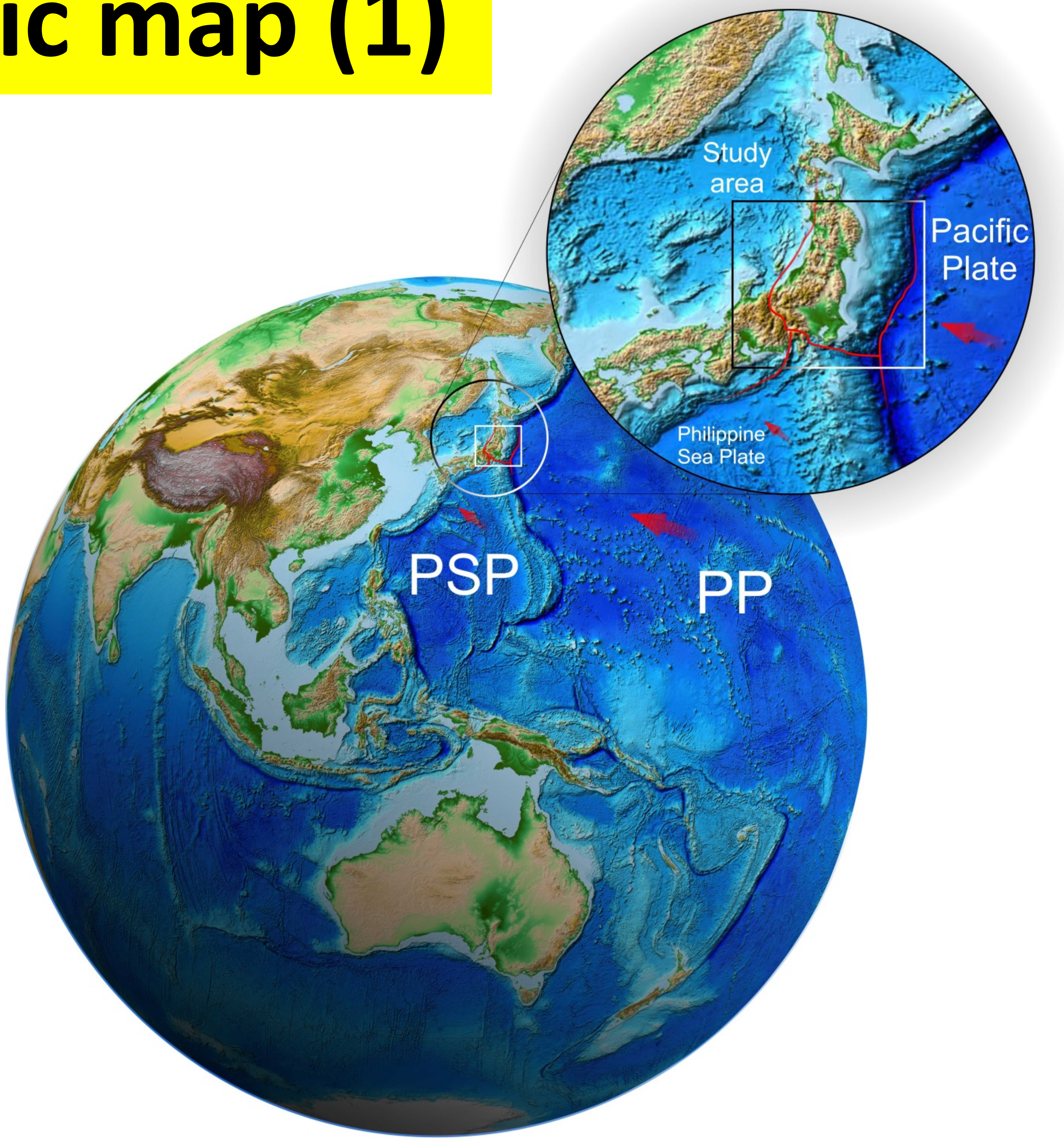

pine

Previous study (1)

- 2-D model

  Iwamori (EPSL, 2000)

  Yoshioka et al. (GJI, 2015)

- 3-D model

  Wada and He (GRL, 2017)

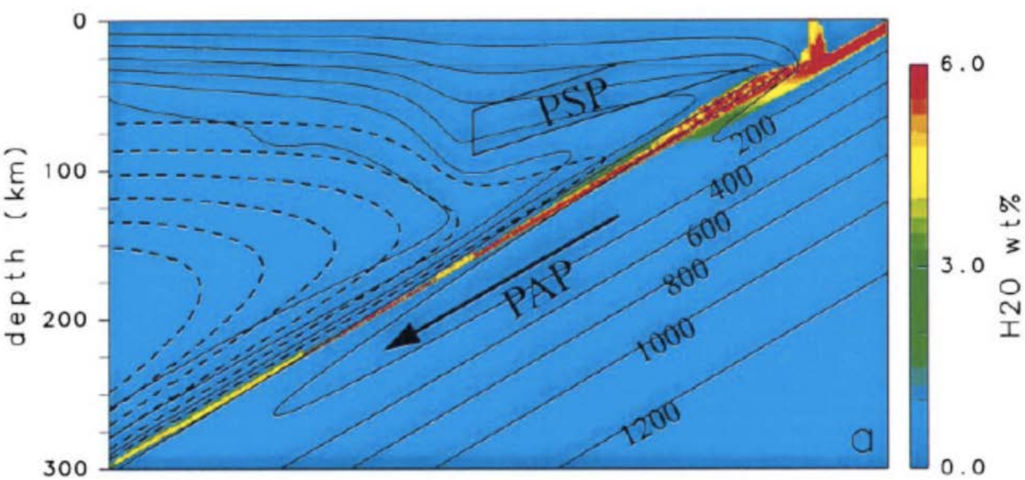

Iwamori (EPSL, 2000)

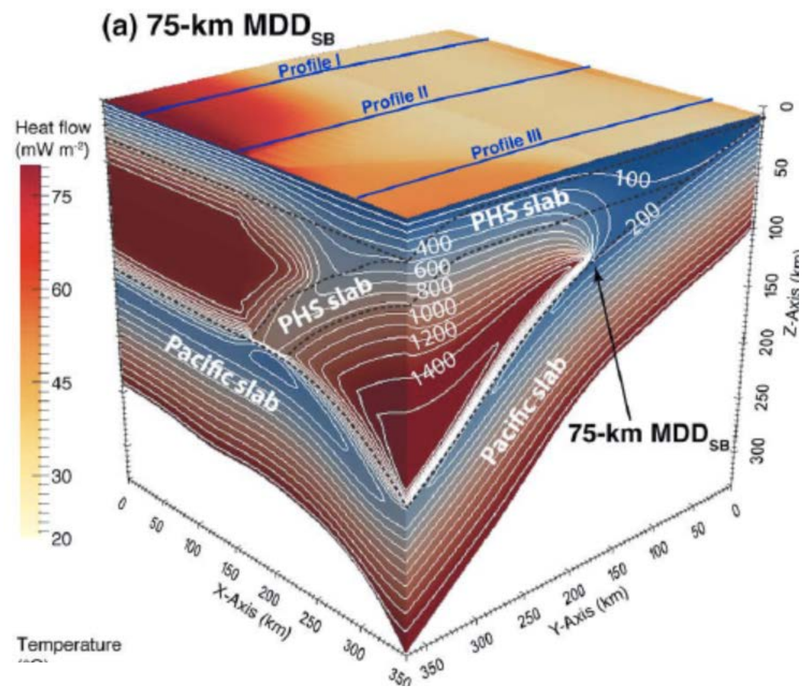

Wada and He (GRL, 2017)

Previous study (2)

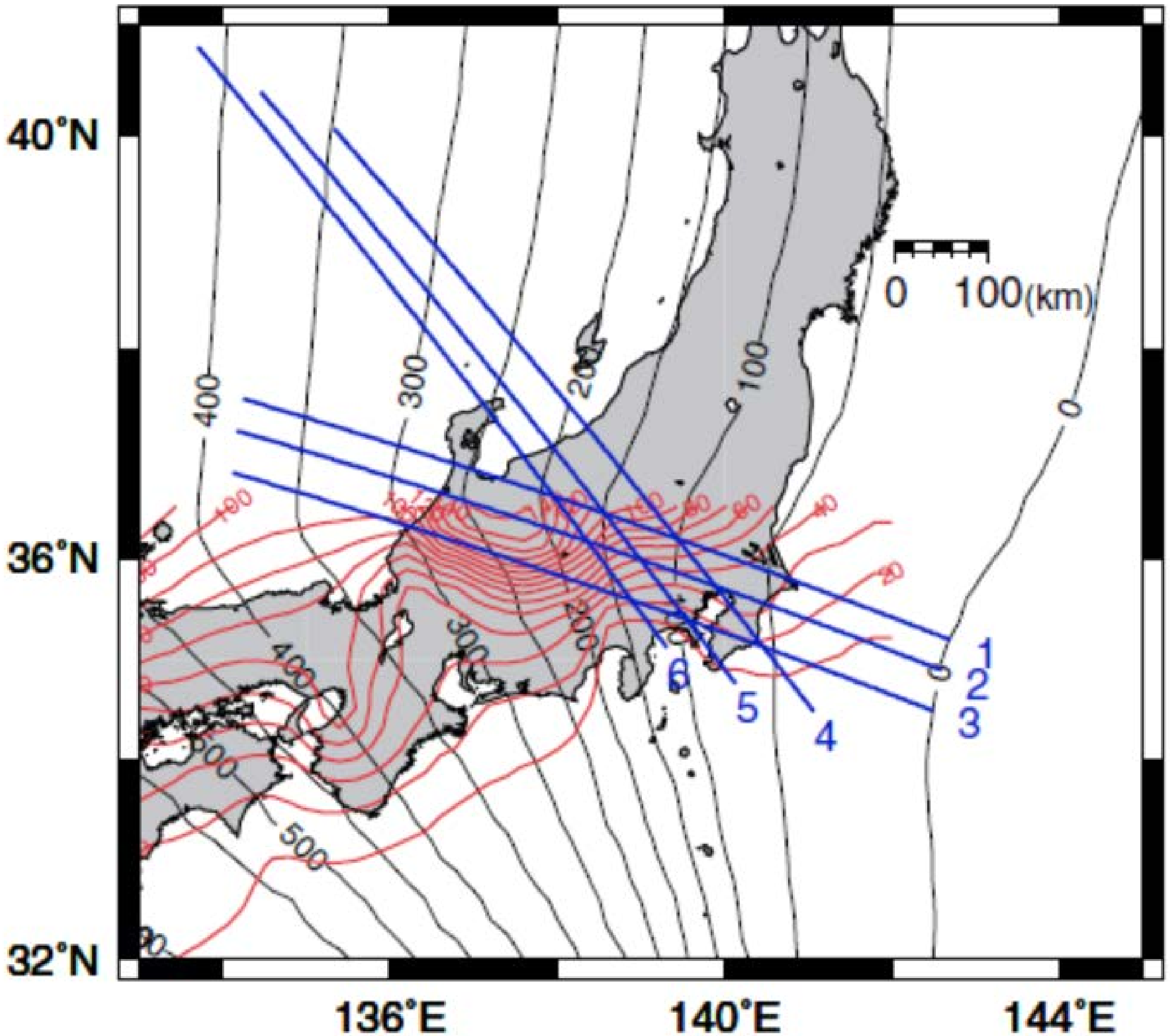

Yoshioka et al. (GJI, 2015)

Previous study (3)

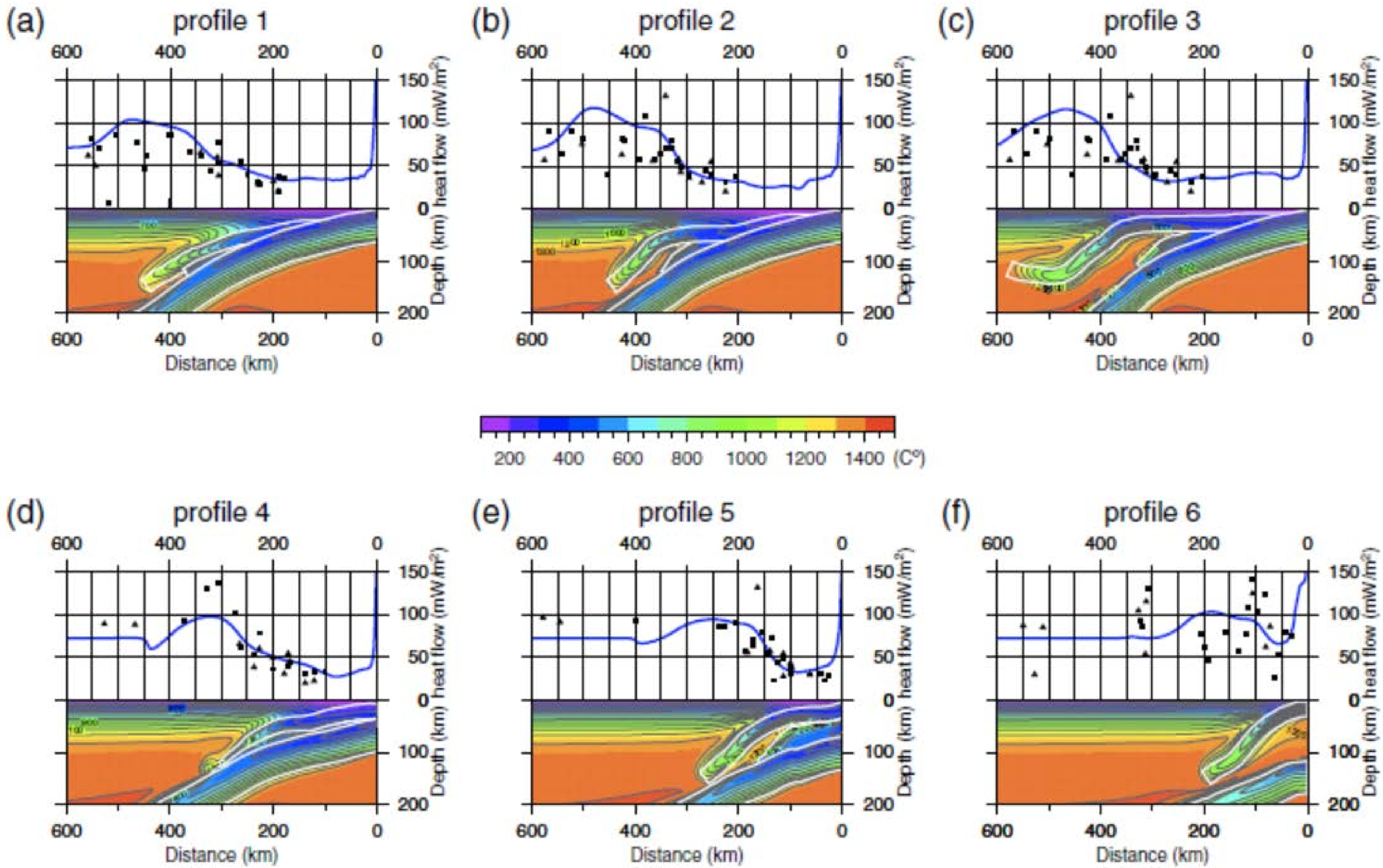

Yoshioka et al. (GJI, 2015)

Necessary data for model construction

- Slab geometry
- Age of the oceanic plates at the Trench or Trough
- Subduction history
- Heat flow

Previous study (3)

temperature

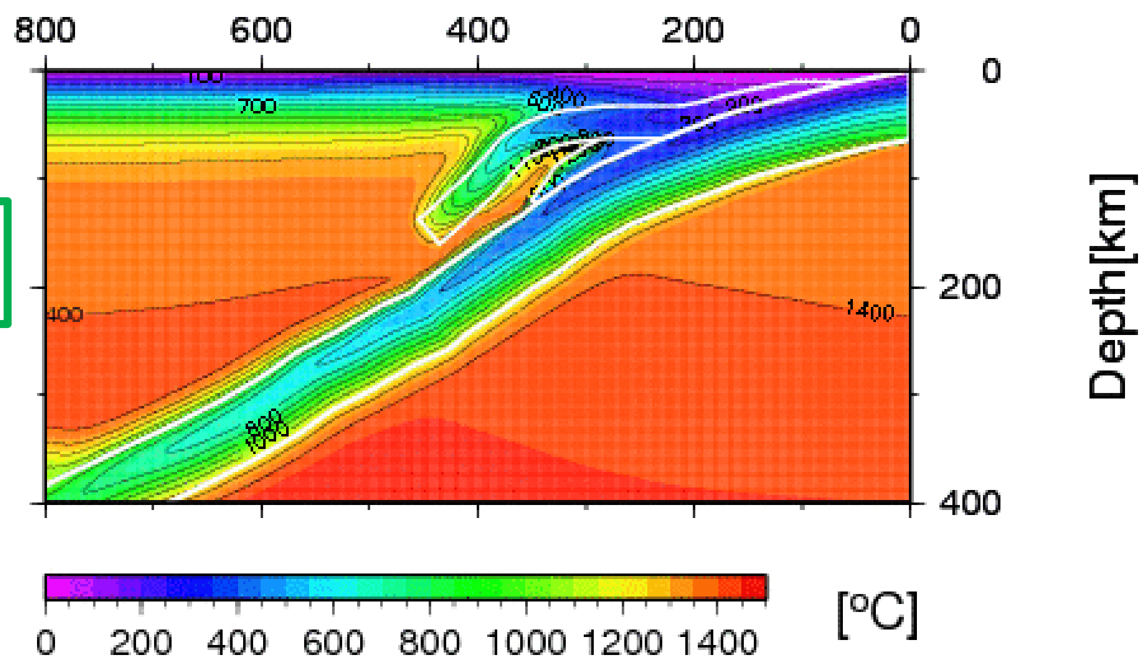

stream function

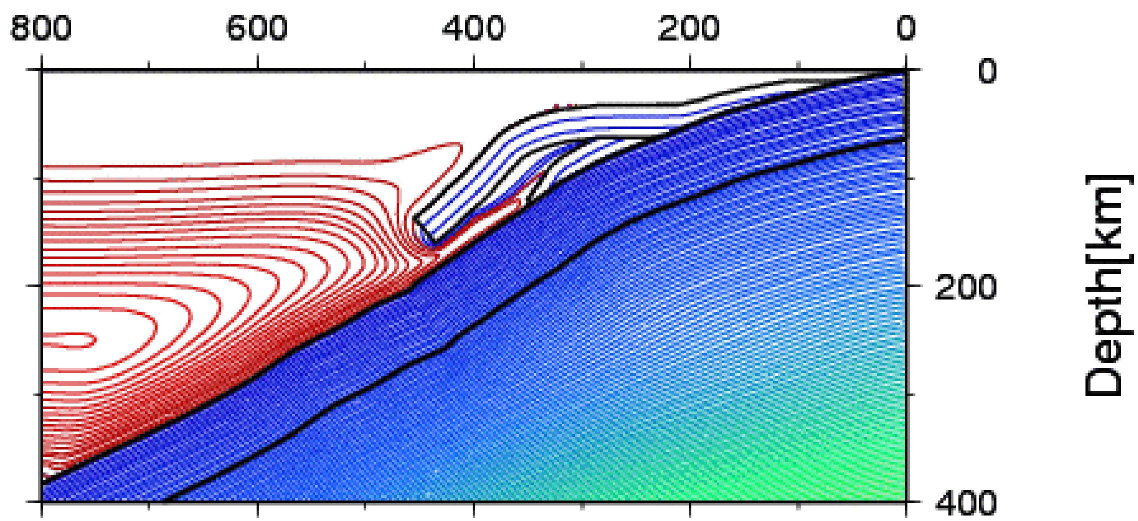

clockwise rotation

anti-clockwise rotation

Yoshioka et al. (GJI, 2015)

Tectonic map (1)

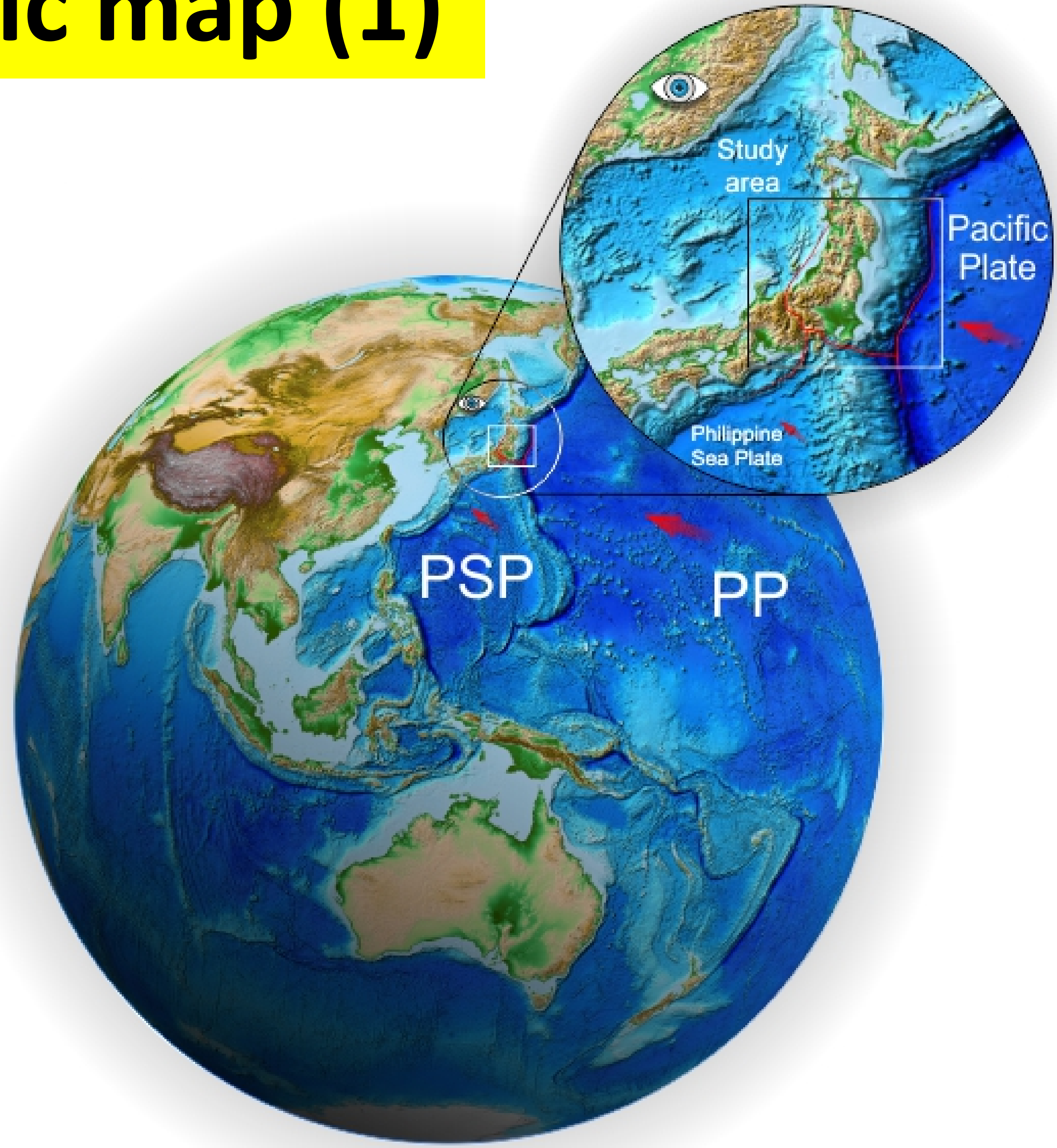

Objectives

・To understand geodynamic process associated with subduction of two oceanic plates beneath Kanto, using 3-D thermal convection subduction model

- **Thermal structure associated with subduction of plates with 3-D complex geometry**
- **Spatial distributions of maximum solubility and dehydration**
- **Mantle flow in the mantle wedge**

↓

To elucidate seismogenesis of inter- and intra-plate earthquakes (≧M2) beneath Kanto

Plate geometry model and distribution of interplate microearthquakes in the study area

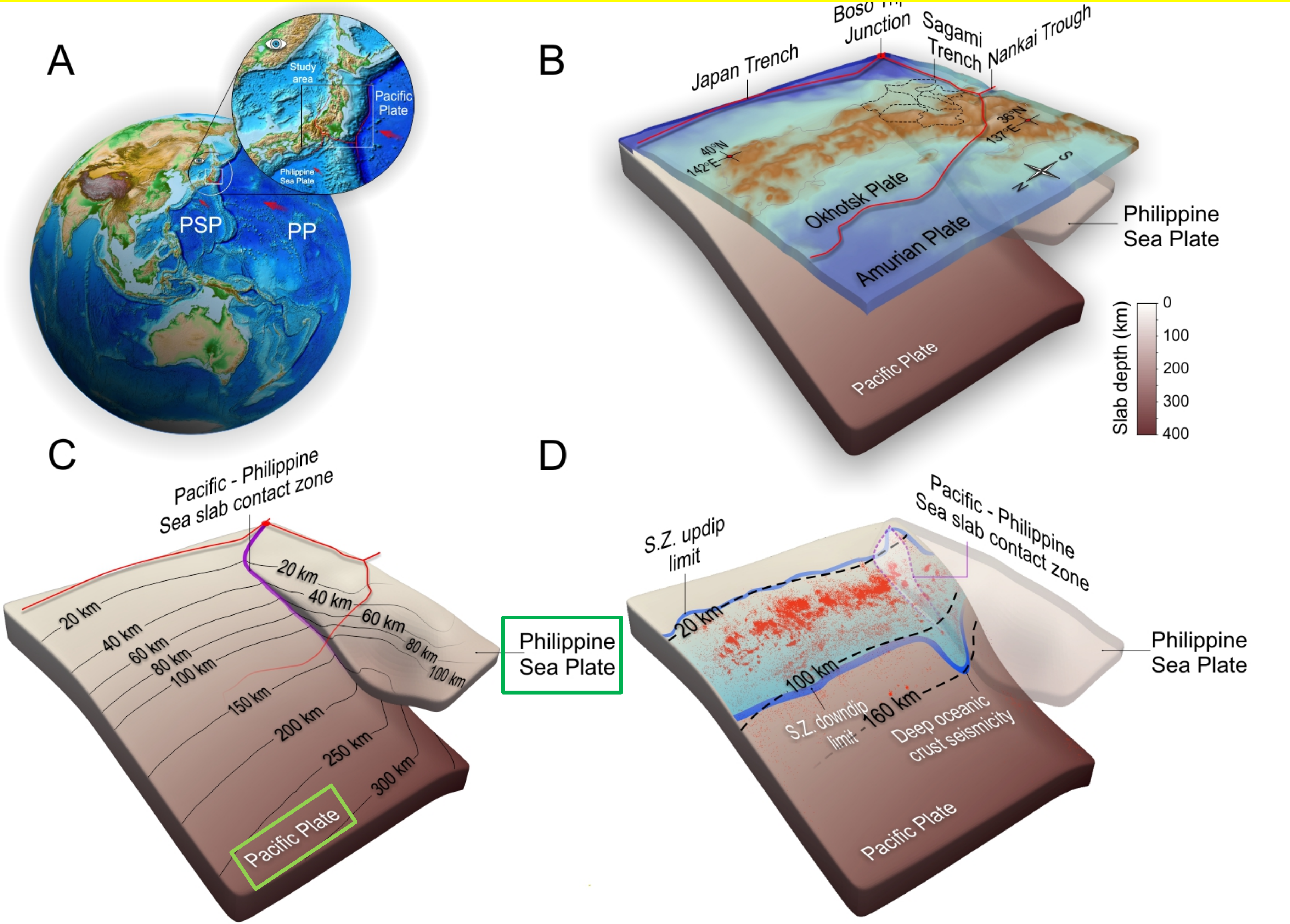

temperature

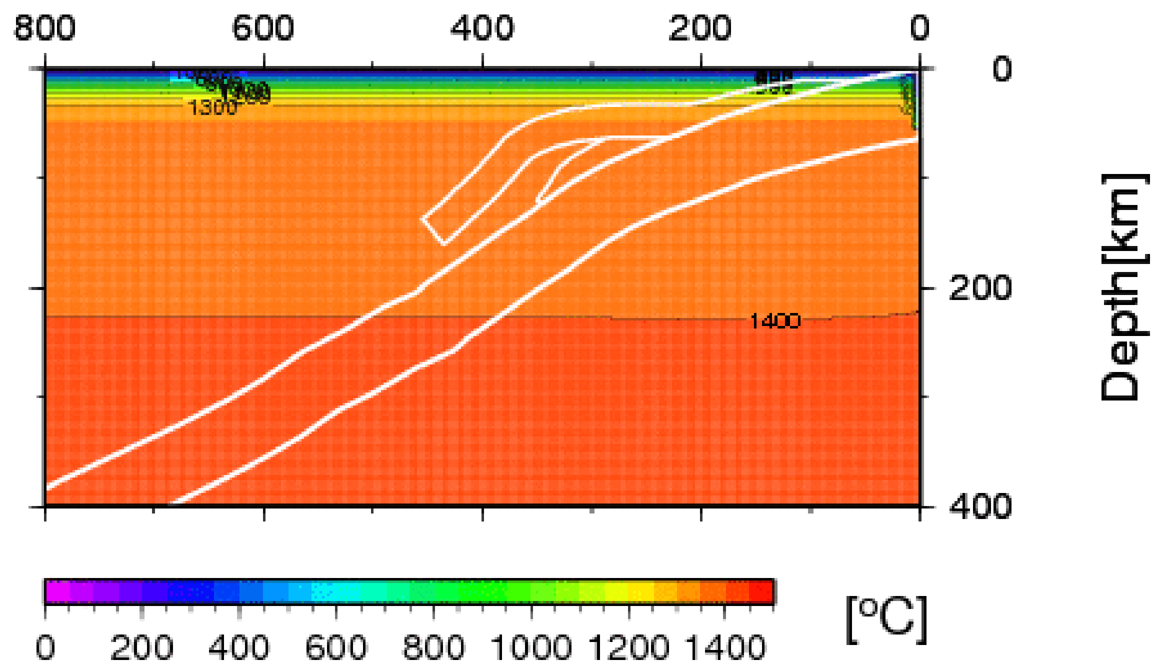

stream function

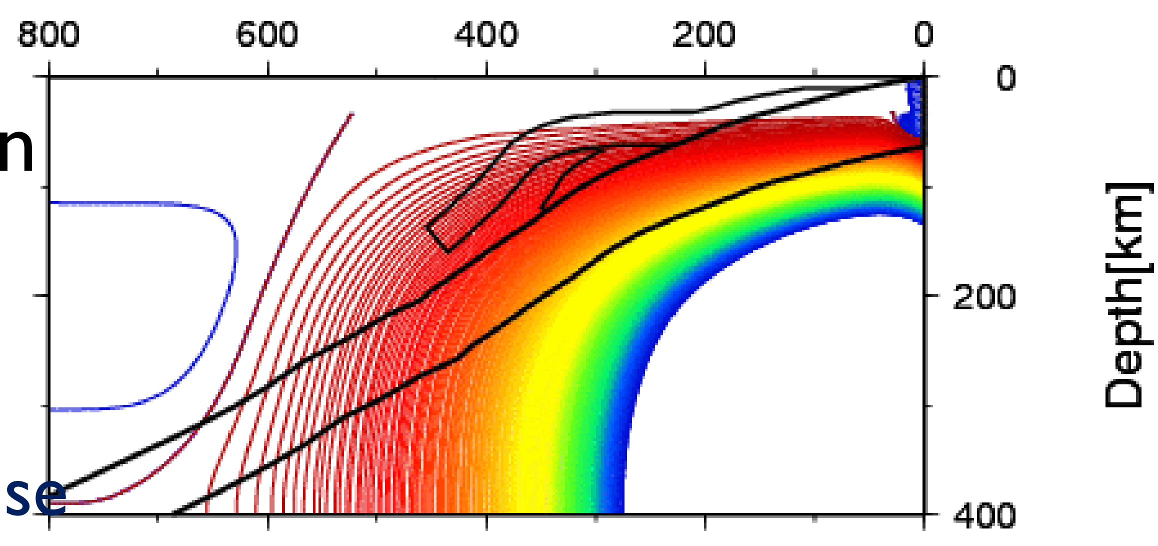

clockwise rotation

anti-clockwise rotation

Yoshioka et al. (GJI, 2015)


www.nature.com/scientificreports
SCIENTIFIC REPORTS

OPEN

Seismogenesis of dual subduction beneath Kanto, central Japan controlled by fluid release

Yingfeng Ji[1], Shoichi Yoshioka[1,2], Vlad C. Manea[3,4] & Marina Manea[3,4]

Received: 28 June 2017
Accepted: 16 November 2017
Published online: 04 December 2017

Dual subduction represents an unusual case of subduction where one oceanic plate subducts on top of another, creating a highly complex tectonic setting. Because of the complex interaction between the two subducted plates, the origin of seismicity in such region is still not fully understood. Here we investigate the thermal structure of dual subduction beneath Kanto, central Japan formed as a consequence of a unique case of triple trench junction. Using high-resolution three-dimensional thermo-mechanical models tailored for the specific dual subduction settings beneath Kanto, we show that, compared with single-plate subduction systems, subduction of double slabs produces a strong variation of mantle flow, thermal and fluid release pattern that strongly controls the regional seismicity distribution. Here the deepening of seismicity in the Pacific slab located under the Philippine Sea slab is explained by delaying at greater depths (~150 km depth) of the eclogitization front in this region. On the other hand, the shallower seismicity observed in the Philippine Sea slab is related to a young and warm plate subduction and probably to the presence of a hot mantle flow traveling underneath the slab and then moving upward on top of the slab.